CHALMERS

STUDY OF SUPPLEMENTARY CONTROLS FOR EMBEDDED HVDC LINKS IN AC POWER SYSTEMS

Thesis for the Degree of Master of Science

HECTOR ARMANDO AVILA R.

Department of Energy and Environment
Division of Electric Power Engineering
CHALMERS UNIVERSITY OF TECHNOLOGY
Göteborg, Sweden, 2008

STUDY OF SUPPLEMENTARY CONTROLS FOR EMBEDDED HVDC LINKS IN AC POWER SYSTEMS

HÉCTOR ARMANDO AVILA RODRÍGUEZ

Examiner: Dr. Tuan Le. CTH
Supervisor: Dr. Gabriel Olguin. ABB Corporate Research

Department of Energy and Environment
Division of Electric Power Engineering
CHALMERS UNIVERSITY OF TECHNOLOGY
Göteborg, Sweden 2008

Study of Supplementary Controls for Embedded HVDC Links
in AC Power Systems

Master's Thesis 2008:NN

Department of Energy and Environment
Division of Electric Power Engineering
Chalmers University of Technology
SE-41296 Göteborg
Sweden

Tel. +46-(0)31 772 1000

Study of Supplementary Controls for Embedded HVDC Links in AC Power Systems

HÉCTOR ARMANDO AVILA RODRÍGUEZ
Department of Energy and Environment
Division of Electric Power Engineering
Chalmers University of Technology

Abstract

This document reports a comprehensive study of supplementary control schemes for HVDC inter-ties parallel to AC transmission lines in order to reduce electromechanical inter-area oscillations employing a suitable two-area power system. The study includes design procedure and an extensive analysis based upon time domain detailed simulations, developed using PSCAD/EMTDC. Results obtained from two-area power system show how the control over the HVDC inter-tie effectively reduces the electromechanical inter-are oscillations. The supplementary outer control loop of the HVDC link, suitably designed, permits to increase the damping ratio of the system to a safe value, which can not be attained solely using power system stabilizers. Power modulation through the HVDC link effectively reduces electromechanical inter-area oscillations under a wide range of composite static load characteristics. Response is however limited by the value of the voltage index for active power; the compensation loop is functional only when this index is greater than one. The effectiveness of the supplementary control scheme is barely affected by the value of the voltage index for reactive power; these results reduce the modeling considerations of the reactive power characteristics, which in practical circumstances are more variable and depending on several and sometimes unknown factors.

Key words: HVDC Control, AC/DC Interaction, Inter-area Oscillations, Supplementary Control, Static Load Characteristic, Small Signal Analysis.

Acknowledgements

First off, I sincerely would like to thank the Swedish Institute (Svenska Institutet) for the grant of scholarship to start and complete my studies in Sweden. Likewise, I am strongly thankful with ABB Corporate Research for the opportunity of developing my thesis work in such important leading-edge company.

I also would like to express my most truthfully gratefulness to my supervisor Gabriel Olguin for all his invaluable support.

Finally, words are not enough to thank to my beloved family for its unconditional support and advice during these days far away from home. My deepest hope it is to find the way to thank you for all the things that you have given to me.

Contents

1. Introduction

Power systems around the world have been remarkably influenced by new technologies based mainly in the impressive development of the high power switching devices. One of the most important of these devices is the solid state HVDC converter, which has permitted the rapid expansion of the HVDC transmission. Thus, in only approximately 25 years, a grand quantity of HVDC transmission lines has been embedded in diverse power systems around the world [1], [2]. This has created the necessity of understanding the dynamic of the interaction between AC and DC systems. This work centres in this dynamic, particularly in the inter-area oscillation phenomenon and the control aspects needed to improve the dynamic performance of power systems with HVDC links.

Damping of electromechanical inter-area oscillations in large power system has been a challenge for engineers around the world. Numerous studies, not only theoretical [20], [26], and [27] but also practical [17], [28], [29], and [30], have been developed in order to systematically reveal the nature of the oscillations modes and the control methods that can be used to stabilized them. In relation to the nature of the electromechanical inter-area modes, several remarkable conclusions have been established. They included the range of frequencies in which they emerge, and their dependency with the system structure, operating conditions, control systems of the generators, and system loads. Likewise, in relation to the control methods, mainly three feasible solutions have been stated; namely, the installation and coordination of power system stabilizers, the use of the properties of the HVDC links embedded in the power systems, or the use of FACT devices [21]. One of the aims in this work will be to combine and to study the first two methods mentioned before, applied to a study system in order to evaluate their effectiveness in the damping of electromechanical inter-area oscillations.

In the case of the theoretical studies referred above, it has been outstanding the results reported about inter-area oscillations phenomenon based on the extensive evaluation of a simple two are system [7], [27]. Most of the work reported here will be developed using the same two area system but focusing mainly in the possibilities of an additional HVDC link and considering a more realistic system including power system stabilizers, which are important part of the real power networks [20].

HVDC links embedded in AC power systems can be controlled in a wide variety of forms by adding supplementary control schemes to the same basic control

structure. The purposes of these supplementary control schemes are multiple and in general they have been developed to satisfy the particular conditions of each HVDC project [10], [11], and [14]. Therefore, there is no a general control scheme applicable to all systems. Specifically in this work, for instance, a supplementary control loop acting over a DC inter-tie of a typical two area study system will be designed and tested. The purpose of this supplementary control structure associated to the HVDC link will be to improve the damping of the system overall. Tests over the compensation scheme designed will include different disturbances and a detailed study of the load characteristics. The importance of the load characteristics and their influence in the power system analysis and in particular in the electromechanical inter-area oscillations phenomenon have been widely reported [27], [34]. Due to this fact, variations on load characteristics will be included in the evaluation of the supplementary control system.

All the analysis of the different aspects mentioned above will be made in time domain using the widely known platform PSCAD/EMTDC [32]. The design procedure of the supplementary control system will be developed using a specialized tool useful for small signal stability analysis, namely MagNetEig [26].

1.1. Report Outline

A brief description of each chapter in this report is given below:

Chapters 2 and 3 summarize the basic concepts of HVDC systems and their interaction with AC systems. Chapter 4 is entirely dedicated to explain the main characteristics of the control of HVDC links. Chapter 5 presents a succinct description of the small signal stability analysis and the theoretical fundaments of the method employed to design the supplementary control block. Chapter 6 describes the nature of inter-area oscillations and details the study system used. In chapter 7, a detailed description of the modelling of the study system in PSCAD/EMTDC is presented. Chapter 8 shows the design procedure of the supplementary control loop applied to the study power system. Chapter 9 describes the simulations results along with a detailed analysis. Chapter 10 presents the main conclusions obtained.

2. HVDC conventional systems

An increasing necessity around the world for transmitting huge energy quantities through long distances has pushed the development of a new technology based upon power electronics systems. The new technology is the transmission of energy using direct current or shortly HVDC and the power electronic systems are different types of converters whose main component is a highly efficient switching device. Even though, transmission using DC has been implemented since nineteenth century [1], only in last fifty years its potential has been explored and exploited, hence the denomination of "new".

HVDC systems are nowadays divided in two big branches considering the technology used in the conversion stations of the system. Conventional systems or classic systems refer to those HVDC systems based firstly on mercury-arc valves in early applications and subsequently those developed using thyristors. On the other hand, HVDC systems with voltage source converters (VSC), whose basic component is the insulated gate bipolar transistor (IGBT) or gate turn-off thyristor (GTO), conform the second branch. In this work only conventional systems are considered.

2.1. Six-Pulse Bridge Converter

The basic unit of a converter station in a conventional HVDC system is the six-pulse bridge converter or so called Graetz bridge [1], [2]. The structure of the bridge is shown in the Figure 2-1.

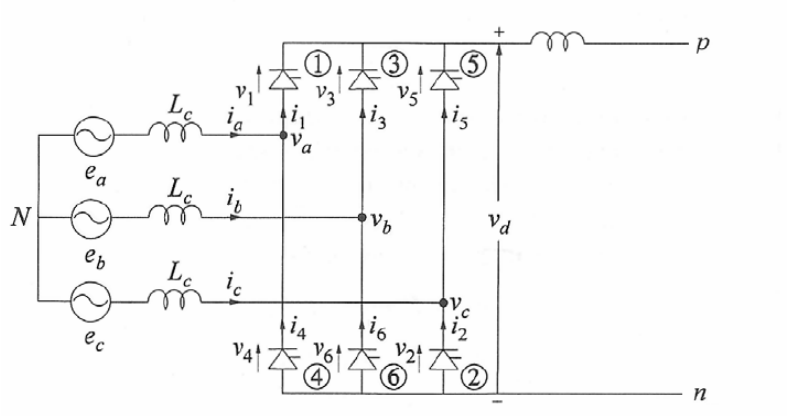

Figure 2-1: *Graetz bridge.*

An AC-three phase balanced system is connected to the bridge, which consists of six valves. Valves, normally thyristors, can be controlled deciding the instant of conduction. The operation of the bridge rests in the fact that thyristors conduct in associated pairs and the commutation between valves is determined by the AC phase voltages. Referring to the Figure 2-1 the pairs mentioned correspond to valves 1 and 2, valves 3 and 4, and valves 5 and 6.

If a continuous control signal is applied to the thyristors, their behavior is similar to diodes. In that case, called natural conduction state, and considering in addition instantaneous commutation, the output voltage will be a six-pulsed signal. Typical voltage waveforms for this condition are depicted in Figure 2-2.

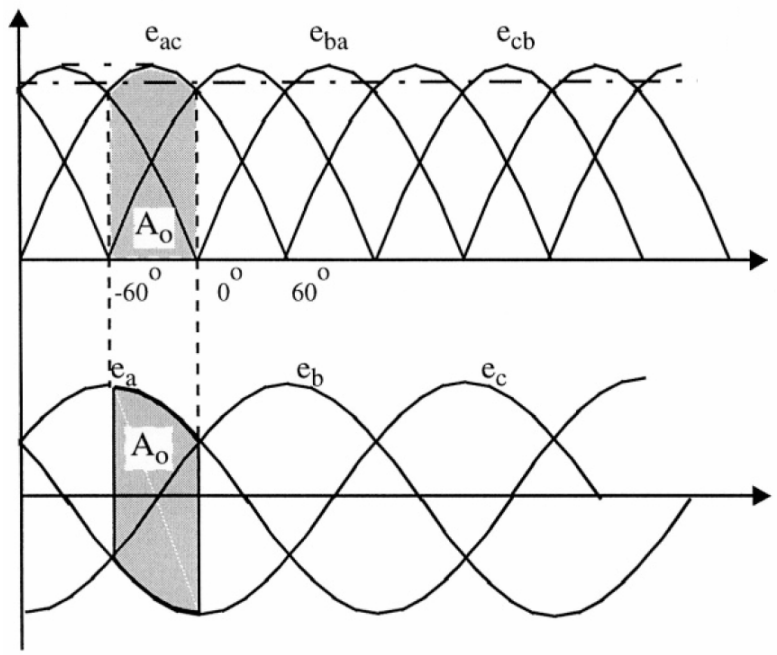

Figure 2-2: *Voltage waveforms for the natural conduction state case [2].*

The average of the ideal no load DC voltage V_{d0} is given by [3]:

$$V_{d0} = \frac{3\sqrt{2}}{\pi} e_{LL} \qquad (2\text{-}1)$$

where e_{LL} corresponds to the rms value of the AC phase to phase voltage applied to the converter.

However, versatility of the six-pulse bridge is only evident when the thyristors are controlled injecting suitable trigger pulses. In this way the conduction times of the valves are fixed and certain delay angle with respect to the natural conduction state is obtained and consequently the average DC voltage is changed.

This delay angle or firing angle is termed α. Figure 2-3 shows the effect of the firing angle over the output voltage waveform.

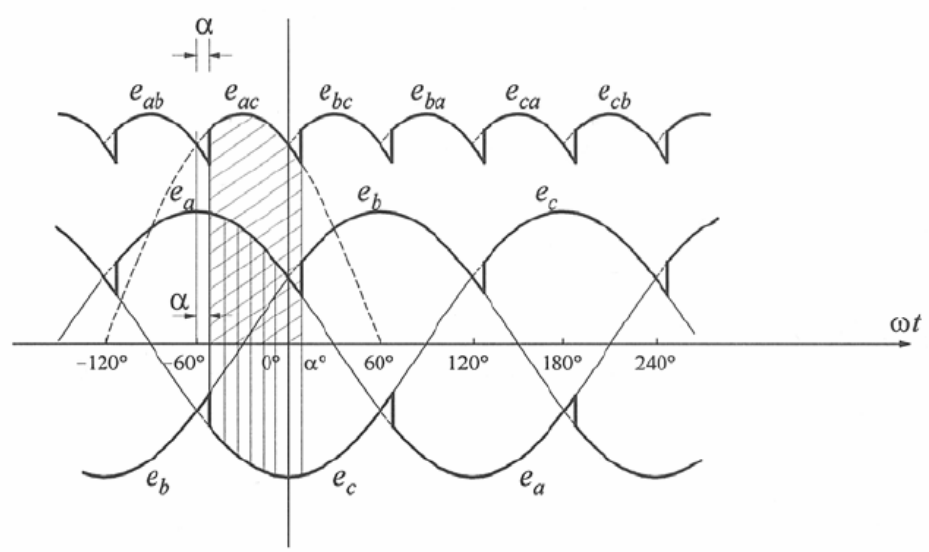

Figure 2-3: *Voltage waveforms with a delay angle.*

Variation of the output DC voltage in relation to the firing angle is shown in the equation (2-2).

$$V_d = V_{d0}\cos\alpha - \frac{3X_c}{\pi} I_d \qquad (2\text{-}2)$$

The commutation reactance X_c in the foregoing equation is associated to the inductance L_c of the AC source (see Figure 2-1). This inductance corresponds generally to the leakage inductance of the converter transformer that supplies the AC voltages [1].

An important practical relation for this converter is its consumption of reactive power. In terms of the active power it can be expressed as [1]:

$$Q = P\tan\phi$$

$$\cos\phi \approx \cos\alpha - \frac{3X_c I_d}{\pi V_{d0}} \qquad (2\text{-}3)$$

Hence the reactive power depends on the load conditions and also on the firing angle. In order to keep the power factor of the converter in acceptable values is necessary to reduce the firing angle as much as possible. Normally α is maintained in the range of 15 to 20 degrees.

One remarkable feature of the six-pulse bridge is that it can be operated not only as a rectifier as has been described above, but it also can be operated as an

inverter. In order to achieve that, the firing angle is increased over 90 degrees but below 180 degrees. Due to this it is common to describe expressions for the inverter in terms of the extinction angle γ instead of the firing angle. Extinction angle is defined as:

$$\gamma = \pi - \mu - \alpha \tag{2-4}$$

Where μ represents the overlap angle [1]. The expression for the DC voltage at the inverter, for instance, is normally stated as:

$$V_d = V_{d0}\cos\gamma - \frac{3X_c}{\pi} I_d \tag{2-5}$$

2.2. HVDC Typical Components and Configurations

High voltage direct current systems are based in the Graetz's bridge described in section 2.1 and their operation embrace one simple idea. Generated AC power is converted to DC and transmitted in this condition over a DC line to another converter, which conversely return power again to AC. Even though, several different configurations have been developed in order to accomplish this purpose, a few basic components are common to those configurations. Figure 2-4 depicts a bipolar HVDC transmission system including its main components.

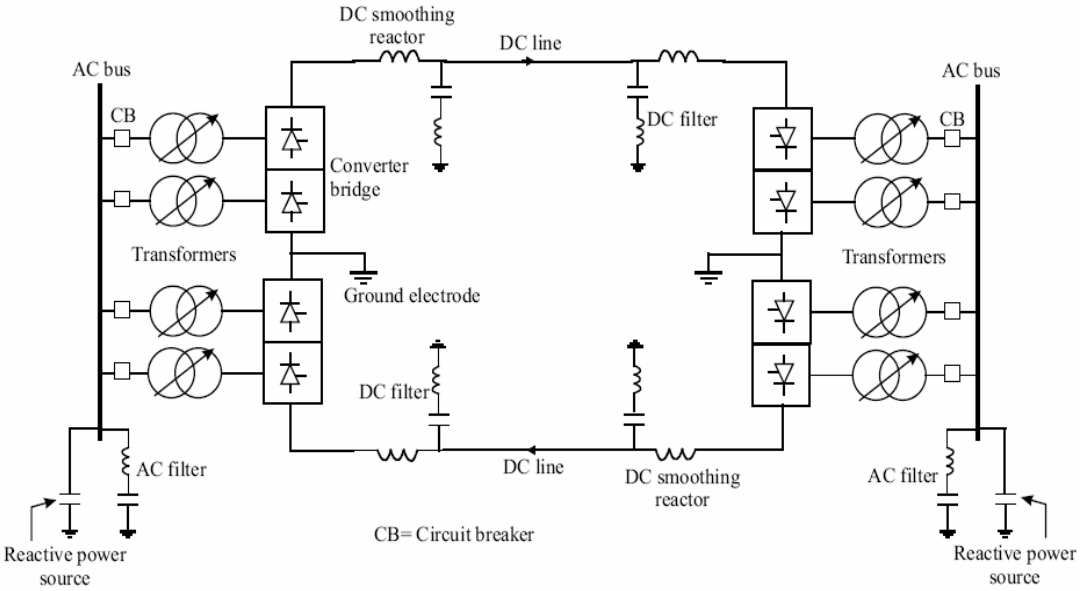

Figure 2-4: *HVDC bipolar configuration [5].*

As can be seen in the figure, six-pulse bridges are connected in series with the intention of handle higher voltage levels. The most common arrangement for the converter station is the twelve-pulse converter, which is compounded of a pair of six-pulse bridges connected in series. A detailed representation is depicted in the Figure 2-5. Each single converter is fed by an independent transformer. These transformers, named converter transformers, are identical, but with different connections in their windings. The purpose is to achieve a shift of 30 degrees in the AC voltages. Normally one of them is wye-wye connected while the other one is wye-delta connected. With this disposition not only higher voltages can be obtained but also lower harmonic distortions. The phase shift cancels out certain harmonics leaving only those of order 12, 24, 36,…,12n at the DC side of the converter and those of order 11, 13, 23,…,12n±1 at the AC side [4]. Remaining harmonics must be eliminated and for that reason several filters are installed at both sides of the converters (see Figure 2-4).

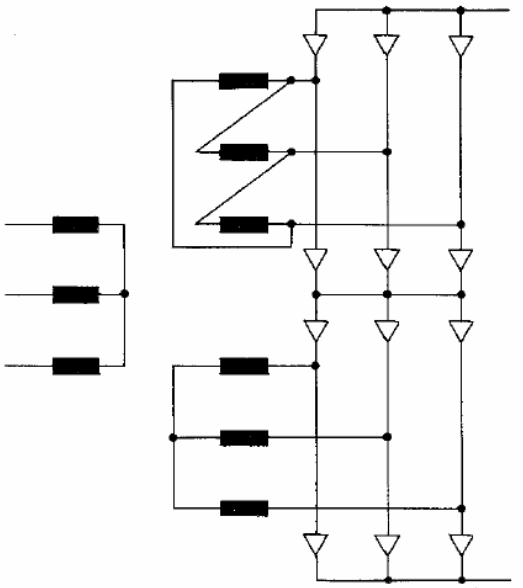

Figure 2-5: *12-Pulse Converter.*

Besides filters, some capacitor banks are also installed in the converter stations. They are used to compensate the reactive power consumption of the converters (see section 2.1), which typically can be around 60% of the active power transmitted [1].

Albeit the bipolar configuration shown in Figure 2-4 is the most widely used in HVDC applications, there is a simpler configuration possible, which uses only one conductor. That configuration is termed monopolar and is illustrated in the Figure 2-6.

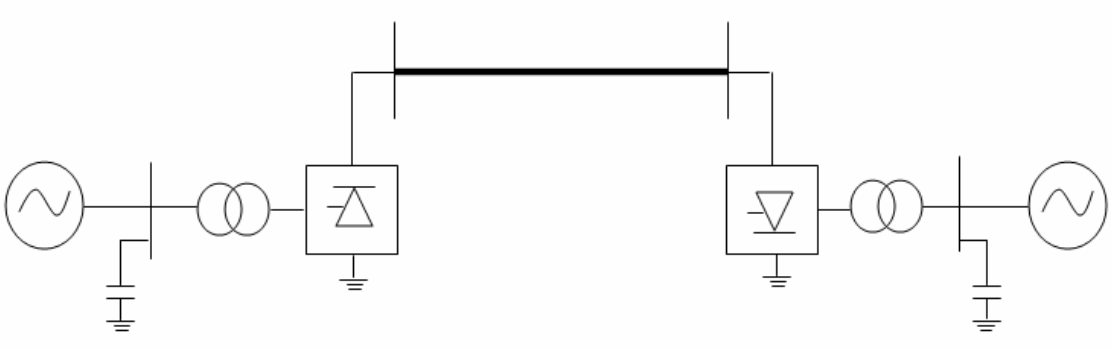

Figure 2-6: *HVDC monopolar configuration with earth return.*

In monopolar configuration the return conductor is normally the earth or the sea. Its application is limited to systems of low power rating [4].

A simple model of a complete monopolar HVDC link interconnecting two AC systems with different nominal frequency is available at the library of SIMULINK-SimPowerSystems [9]. The system is illustrated in the Figure 2-7.

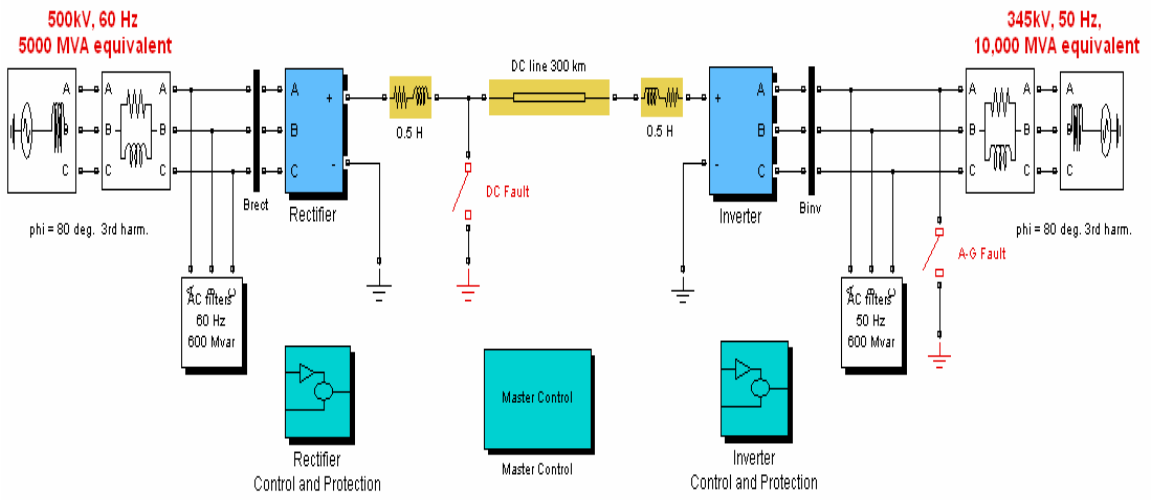

Figure 2-7: *HVDC monopolar system [9].*

The AC systems are represented by damped L-R equivalents with an angle of 80 degrees at fundamental frequency (60 Hz or 50 Hz) and at the third harmonic. The rectifier and the inverter are 12-pulse converters using two 6-pulse thyristor bridges connected in series. Reactive power compensation required by the converters is provided by a set of capacitor banks plus 11th, 13th and high pass filters for a total of 600 MVAr on each side. The HVDC link rated power is 1000 MW at 500 kV.

The response of this simple system is shown in the Figure 2-8. There, it is shown how after the system is started, the rated values for voltage and current are reached. The upper graph, labelled VdL, depicts the DC voltage at the rectifier side. The central graph, labelled Id, shows the DC current circulating in the link. And the lower one represents the behaviour of the firing angle in the rectifier. When the steady-state is settled this angle remains close to 17 degrees. These types of curves are typical for HVDC links.

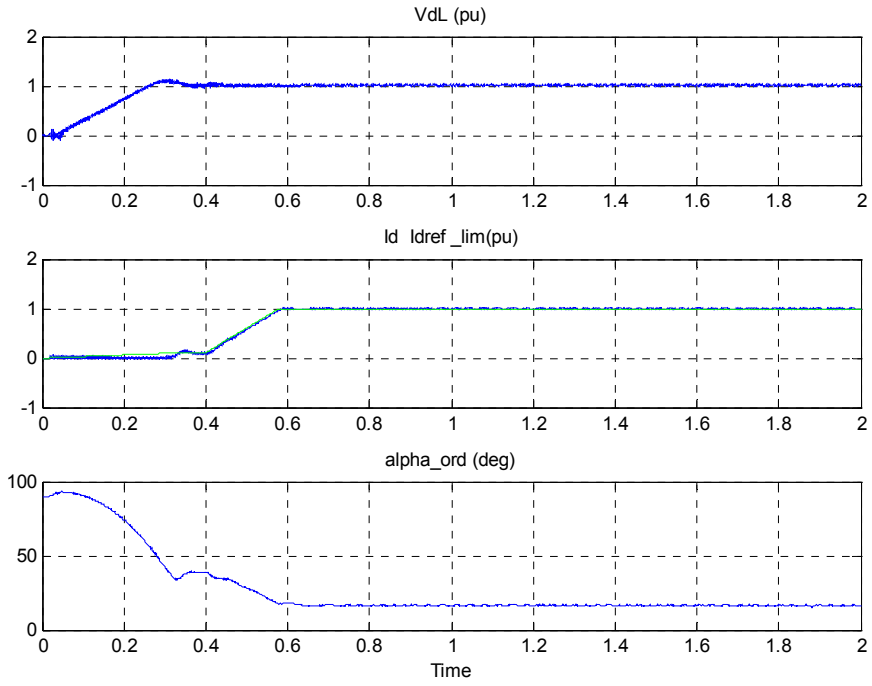

Figure 2-8: *Responses of the HVDC monopolar link of Figure 2-7.*

Another interesting configuration of the HVDC systems is denominated back to back. Its arrangement is depicted in the Figure 2-9.

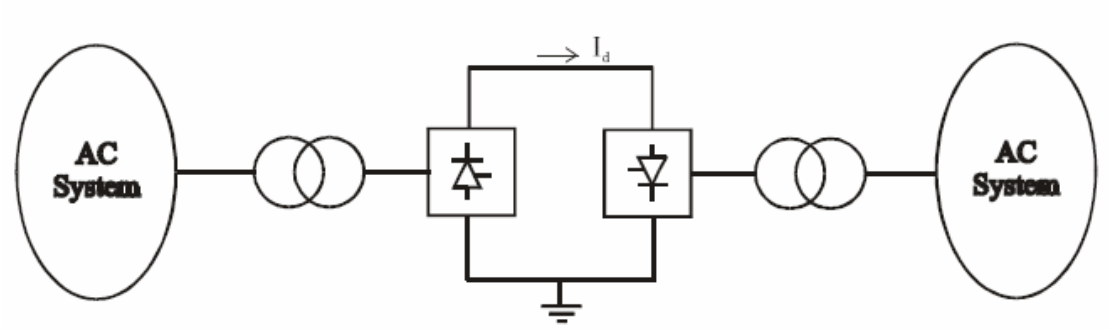

Figure 2-9: *Back to back HVDC system.*

This configuration does not have a DC line that interconnects the two converter stations. Instead, both stations are located in the same place. The purpose of this type of system is to provide an efficient link between two AC systems with different fundamental frequencies or with incompatible control schemes.

3. AC-DC interaction

Nowadays an increasing number of power networks around the world have integrated HVDC systems. Hence a dynamic interaction between the two types of systems emerges. The nature of this interaction is complex and in some cases not totally understood. However, many of the main aspects have been studied and somehow classified.

The basic AC/DC interaction phenomenon is related to electromechanical and quasi steady-state dynamic [6]. As has been stated in section 2.1, converters consume reactive power in the process of transforming power from AC to DC and vice versa. Hence the converter transient response has an impact on generator angles, through active power, and also on system voltages, through reactive power. Thus HVDC systems can influence not only the electromechanical oscillation dynamics but also voltage dynamics of the AC power systems in which they are embedded.

Another type of interaction between AC and DC systems is characterized by the magnification of harmonic AC frequencies by the DC system [1]. This harmonic interaction is mainly due to the non-symmetrized valve firing controls in the converters, the non-linear magnetizing effects of converter transformers, and some low order resonances.

The interaction phenomena mentioned above and their associated problems are strongly related to the relative strengths of the AC and DC systems. These strengths are quantified using mainly two parameters [8]. The first of them is the short-circuit ratio (SCR) defined as the ratio between the AC system short-circuit power and the rated DC power of the HVDC system:

$$SCR = \frac{Short\ circuit\ \ MVA\ of\ \ AC\ System}{Rated\ \ DC\ \ Power} \qquad (3\text{-}1)$$

The short-circuit ratio represents the admittance of the system in per unit as a phasor characterized by its magnitude and angle at fundamental frequency. Therefore SCR gives the intrinsic strength of the AC system.

A more precise parameter from the point of view of the HVDC system performance is the effective short-circuit ratio (ESCR). This ratio is defined as the total per unit fundamental frequency admittance as seen by the converter at the high

voltage busbar including AC system and AC filters [8]. In general the magnitude of the ESCR is defined as the difference between the short-circuit ratio and the ratio (qFC) of the reactive power supplied by capacitor banks and filters and the rated DC power of the converter, namely:

$$ESCR = \frac{(Short\ circuit\ \ MVA\ of\ \ AC\ System) - (\mathrm{Re}\, active\ Compensation)}{Rated\ DC\ Power} \qquad (3\text{-}2)$$

According to some authors [7] the strength levels of the AC systems can be classified as:

- High, if ESCR > 3.0
- Low, if 2.0 < ESCR < 3.0
- Very low, if ESCR < 2.0

In the case of the system illustrated in the Figure 2-7, for instance, the ESCR of the AC system at the rectifier side can be obtained from the frequency response measured before the converter. Figure 3-1 shows the magnitude and the angle of this response, which indeed characterizes the impedance of the system for a range of frequencies, namely from 0 to 1500 Hz.

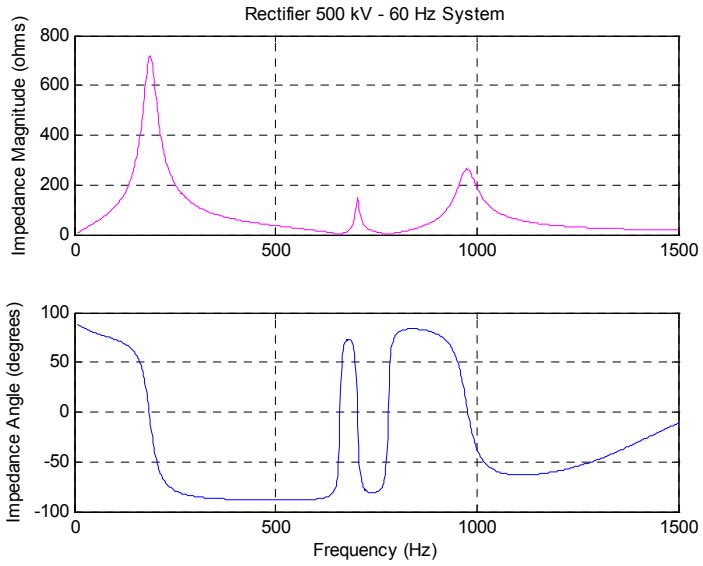

Figure 3-1: *Frequency Response of the HVDC monopolar link of Figure 2-7.*

The impedance of the system obtained from the graph at the fundamental frequency (60 Hz) is:

$$Z(60Hz) = 56.73\angle 78.6^{o}$$

Hence from the equations (3-1) and (3-2) the effective short-circuit ratio for the AC system at the rectifier side is approximately 4.4/-78.6^{o}. Consequently based on the classification described above, the AC system at the rectifier side is a strong system.

4. HVDC control structure

Versatility of the HVDC systems rests not only in the possibility of sending huge energy quantities through long distances or the possibility of interconnecting asynchronous systems but also in the remarkable options derived of its controllability. Some of these options are [7]:

- Improvement of transient stability
- Improvement of damping of electromechanical oscillations between AC systems
- Frequency control of isolated systems
- Reactive power regulation
- Dynamic voltage support

Numerous reported cases show the effectiveness of the HVDC systems to attain those different purposes mentioned before. The project Gezhouba-Shanghai HVDC transmission [10], for instance, is a 1080 km - +/-500 KV bipole line, with 1200 MW rated power. This link connects Central China and East China networks. Under certain operating conditions the two systems can become relatively weak. Hence a reactive power and AC voltage control scheme had to be developed. The control system regulates the reactive power exchange with the AC systems and limits the AC voltage. The reactive power controller is integrated in the DC voltage control loop of the basic control scheme. Other example is the Itaipu HVDC transmission system. The system is a 2-bipole, +/-600 KV link with full capacity of 6300 MW. It connects Foz do Iguacu and Ibiuna substations in Brazil. Supplementary controls are used in the Itaipu HVDC link to improve transient performance of the dc link and dynamic performance of the ac interconnected systems (50 Hz and 60 Hz). For instance, a frequency controller is used to re-establish the generation-load equilibrium when a machine is lost in the 50 Hz generation station [10].

A functional diagram considering the general structure of the control system of an HVDC station is depicted in the Figure 4-1. Although several different representations are possible for each functional block, the structure of the control and its hierarchy are maintained [11]. Each converter station is controlled by the firing angle generated in the current regulator (CR) block. This block is fed by the measured DC current and a current order produced by the current order regulator (COR). The COR adjusts its output signal based on the current order created by the central control regulator (CCR) and the measured DC current at the converter. The

main input to the CCR or master control is the power order, which represents the desired power through the HVDC link. This power order can be modulated using the power-frequency regulator (DCR), which is fed by the suitable measured quantities through the power-frequency measuring regulator block (FPD).

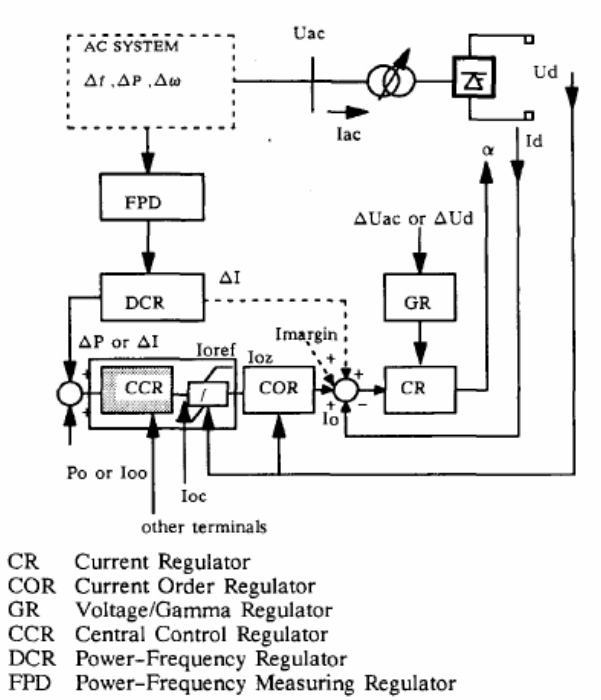

Figure 4-1: *Typical DC Controls Structure [11].*

Next few sections will be devoted to explain in some detail the actual form of the basic blocks of the control of HVDC systems shown in Figure 4-1.

4.1. Basic Control Strategy

A simple two terminal monopolar HVDC system is shown in the Figure 4-2.

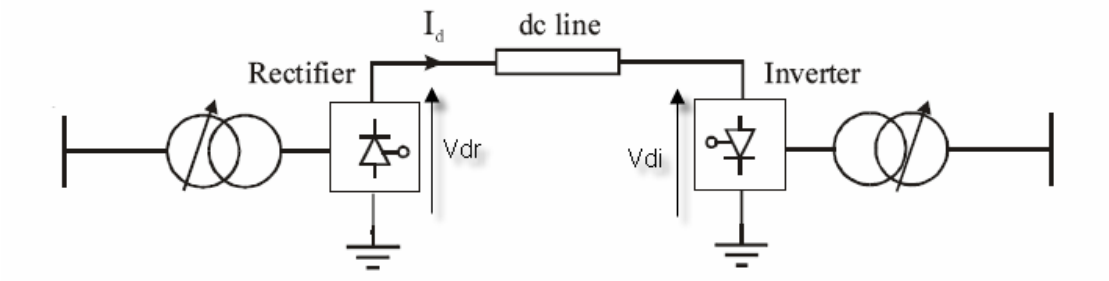

Figure 4-2: *HVDC monopolar system.*

If R_L is the resistance of the line, then the direct current I_d and the power at both sides of line can be found easily as:

$$\begin{aligned} I_d &= \frac{V_{dr} - V_{di}}{R_L} \\ P_{dr} &= V_{dr} I_d \\ P_{di} &= V_{dr} I_d - R_L I_d^2 \end{aligned} \qquad (4\text{-}1)$$

Replacing the equations (2-2) and (2-5) in the expression of the direct current in (4-1), the next result is found:

$$I_d = \frac{V_{dor}\cos\alpha - V_{doi}\cos\gamma}{R_L + \frac{3}{\pi}\left(X_{cr} - X_{ci}\right)} \qquad (4\text{-}2)$$

Expression (4-2) permits to represent the two terminal monopolar system in a simple equivalent circuit. Defining the converter resistances as:

$$\begin{aligned} R_{cr} &= \frac{3X_{cr}}{\pi} \\ R_{ci} &= \frac{3X_{ci}}{\pi} \end{aligned} \qquad (4\text{-}3)$$

then equivalent circuit can be represented as in Figure 4-3.

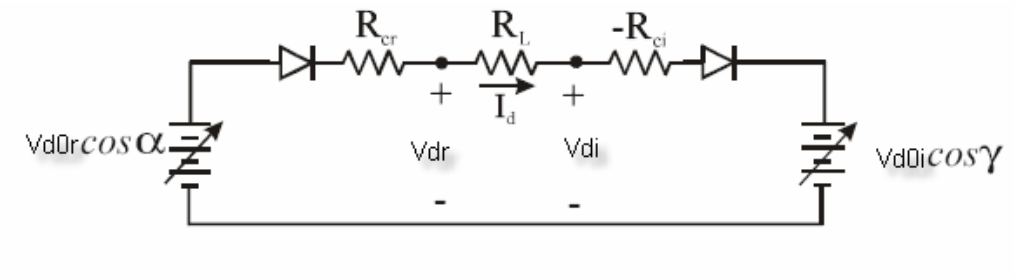

Figure 4-3: *Equivalent circuit of a two terminal HVDC system.*

A quick look of the equivalent circuit reveals that the direct voltage and the direct current at the line can be set either by controlling the firing (α) and extinction (γ) angles or by controlling the AC line to line voltages (see equation (2-1)). Changes in the ignition angles at the converters are accomplished electronically and consequently can be quite fast (about 10 milli-seconds) [2]. On the other hand, variations of AC line to line voltages, which are performed by the tap changing of the converter transformers, are slow, taking around 5 seconds for each step.

In general, mainly during disturbances, a combine strategy is used to control the HVDC system. Initially a rapid response is obtained from ignition angle controls and then the tap changing is activated to restore converter parameters to their rated values. In this work tap changing control is not considered.

4.2. Basic Control Requirements

In order to achieve an applicable control scheme of the two terminal HVDC systems, some essential requirements must be fulfilled [7]. They are chiefly:

- Prevention of large fluctuations in direct current when variations in AC voltages appear. Considering that the line resistance R_L and the converter resistances (equation (4-3)) are small, it is evident from equation (4-2) that small variations in the voltages V_{d0r} and V_{d0i} cause large changes in the direct current. For instance, a variation of 25% in the voltages can produce an increase of the direct current of 100%. Hence the control structure must prevent these fluctuations.
- Maintaining direct voltage near rated value. Once the transmitted power is set, it is desirable to keep the direct voltage profile along the DC line close to the rated value. In this way losses are minimized because the direct current is also minimized.
- Maintaining power factors at the inverter and rectifier side as high as possible. High power factors represent high rated power of the converter, minimization of losses and current rating of equipment in the AC side, minimization of voltage drops at the AC terminals, and minimization of the cost of reactive power compensation.
- Prevention of commutation failures. Commutation failures produce instabilities in the converter operation; hence control systems must reduce them.
- Limitation of the maximum direct current. Valves in converters have inherently a current limitation, which must be maintained.

With the aim of satisfying the conditions mentioned above, a widely accepted method, called current margin, has been developed [2]. The essence of the current margin method rests on the definition of an operation zone of the DC system with clear separate functions for both terminals. Thus, in general, current regulation is assigned to the rectifier while the voltage regulation is left to the inverter.

4.3. Control Characteristics

Based on equations (2-2) and (2-5) is possible to trace the characteristics in steady state of the direct voltage and the direct current for the two terminal HVDC system. These characteristics define the operation point of the system and several others operation regions. Figure 4-4 sketches a regular complete static characteristic for the two terminal system.

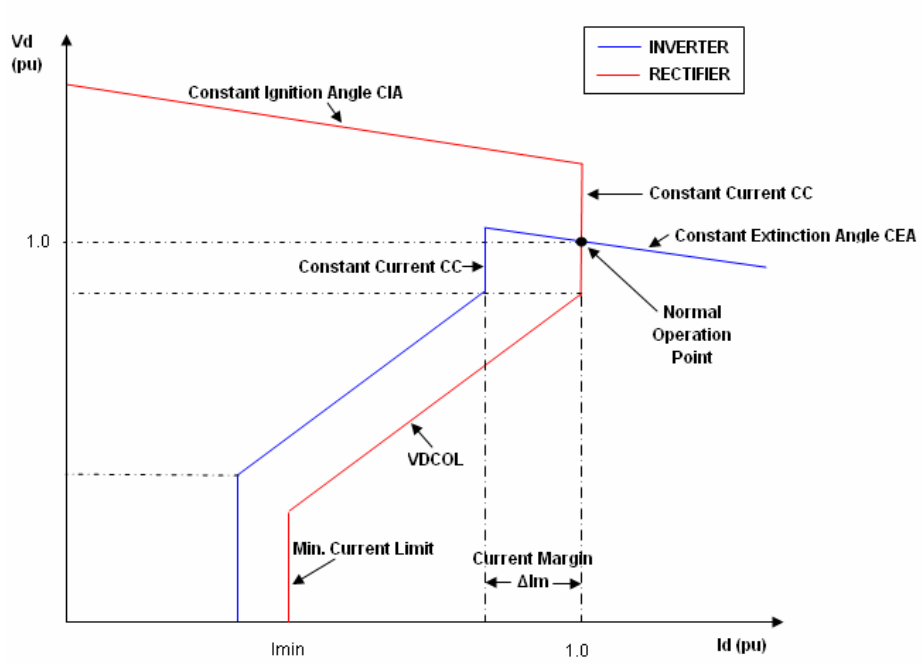

Figure 4-4: *Complete Static V_d-I_d Characteristic for a Two Terminal HVDC System.*

As has been stated before, under normal operation conditions the rectifier maintains constant current (CC) while the inverter operates with constant extinction angle (CEA) maintaining the voltage. Hence an operation state of the two terminal HVDC system must satisfy both conditions for rectifier and inverter; that operation point is defined by the intersection of the characteristics of the terminal converters, (see Figure 4-4).

The red curve (rectifier characteristic) of the Figure 4-4 shows that the constant current condition can be attained changing the firing angle (α) and consequently increasing the DC voltage. However, this variation is limited by a minimum ignition angle (α_{min}), required to ensure the converter valves have a minimum positive voltage for switching on [2]. After this limit is reached no further voltage increase is possible and the rectifier will operate in constant ignition angle (CIA) mode [7].

Similarly, the inverter characteristic (blue curve in the Figure 4-4) illustrates how the constant extinction angle mode (CEA) is maintained. The CEA characteristic intersects the rectifier characteristic to define the operation point. Nonetheless, when the rectifier characteristic is set at reduced voltage, which means a reduction in the rectifier voltage, then a suitable operation point is not reached. Under these circumstances the system would run down. Because of this reason, the inverter characteristic is complemented with a region of constant current (CC) adjusted at a lower value than the current setting of the rectifier. The difference between both settings is called current margin and its value is normally fixed in the range of 10%-15% of the rated current of the system [7]. Subsequently, under reduced voltage condition at the rectifier the role of each converter is switched (mode shift) and thus the rectifier regulates the voltage while the inverter regulates the current.

Referring to Figure 4-4, some current limitations can be observed. First, there is a maximum short time current, which usually becomes in the range 1.2 to 1.3 times the full-load current. This limitation comes from the thermal constrain of the valves in the converters. Secondly, there is a minimum current limit. This minimum limit prevents mainly discontinuities due to the high ripple of low currents.

The third current limitation is associated to low voltage conditions. Under these circumstances it is desirable to reduce the maximum direct current available in order to reduce the reactive power demand and prevent commutation failures [1]. This reduction in direct current is achieved defining a voltage-dependent current order limit characteristic (VDCOL). This type of characteristic is also illustrated in the Figure 4-4, being identical for inverter and rectifier so as to keep the current margin. The VDCOL transiently reduces the direct current based on a piecewise-linear characteristic, which can be a function of the AC commutation voltage or the DC voltage [12]. Some more elaborated methods which use local information at each converter have been developed to model VDCOL and the other parts of the static characteristic [13].

A typical VDCOL implemented in the David A. Hamil (DAH) DC Tie is shown in the Figure 4-5. The system is a 110 MW back to back tie, which interconnects asynchronous systems [14]. The voltage-dependent current order limiter was designed to reduce the reactive power demand on the AC system during periods of reduced voltage. The application of the limit is delayed with a time constant of 0.5 seconds. If the AC voltage drops below 0.5 pu, the system is shut down. Recovery will start for voltages above 0.8 pu and will be delayed 0.2 seconds.

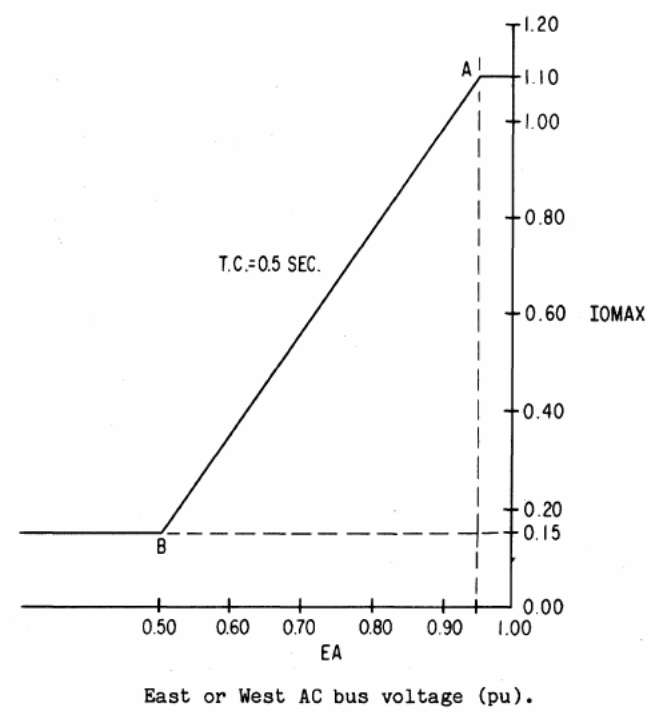

Figure 4-5: *DAH DC Tie Voltage Dependent Current Order Limiter (VDCOL) [14].*

Next section will focus in the implementation of the control system for a two terminal HVDC link based upon main features described above.

4.4. Cigre Benchmark Model

To facilitate the understanding of the control structure a special two terminal HVDC system and its basic control have been implemented in SIMULINK [9]. Afterwards some simulations have been run and its results are presented. A complete report of the results can also be found in [15].

The special system, mentioned before, is a benchmark model of a monopolar two terminal HVDC transmission system, which has been developed by CIGRE [8]. The model has been elaborated for comparative studies of different HVDC control schemes. All the parameters of the system are detailed including component values, ratings, operation conditions for converters, and steady state conditions.

The CIGRE benchmark system consists of a 500 kV - 1000 MW - DC link, which connects two 345 kV and 230 kV AC systems, Figure 4-6. Each AC system has a pre-set Short Circuit Ratio (SCR), which represents the degree of strength of the system. Their values in the rectifier side (345 kV) and in the inverter side (230 kV) are respectively: 2.5pu/-84° and 2.5pu/-75°. The model also considers AC filters of the

damped-arm type and capacitor banks for reactive power compensation. The DC transmission line is considered as a long cable system and hence is represented by a T-section model with high shunt capacitance and low series inductance.

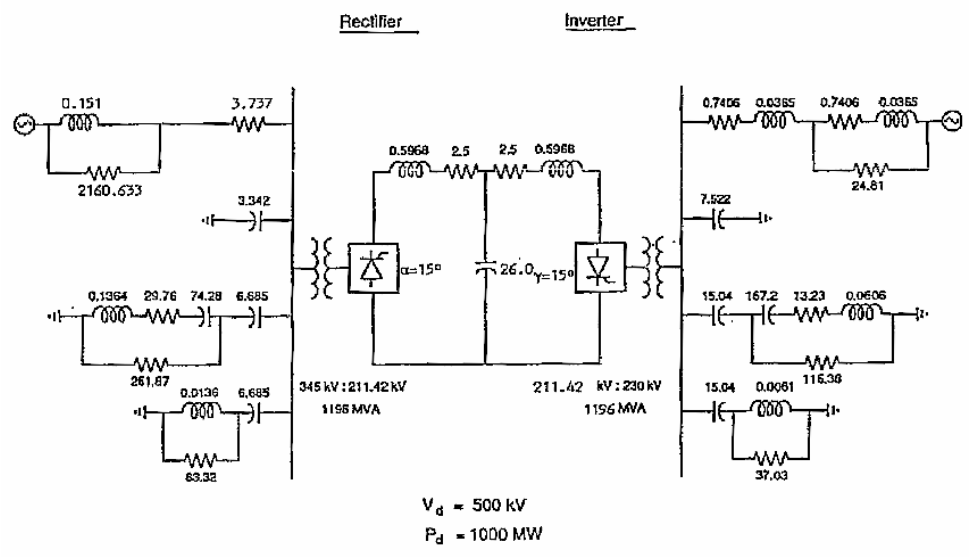

Figure 4-6: *Benchmark model configuration.*

An important characteristic of the model is its frequency impedance response, particularly the magnitude of the positive-sequence impedance measured from AC sides (Figure 4-7). Resonances due to interaction of capacitor banks connected to the highly inductive AC systems can be identified at both sides of the system around 95 Hz.

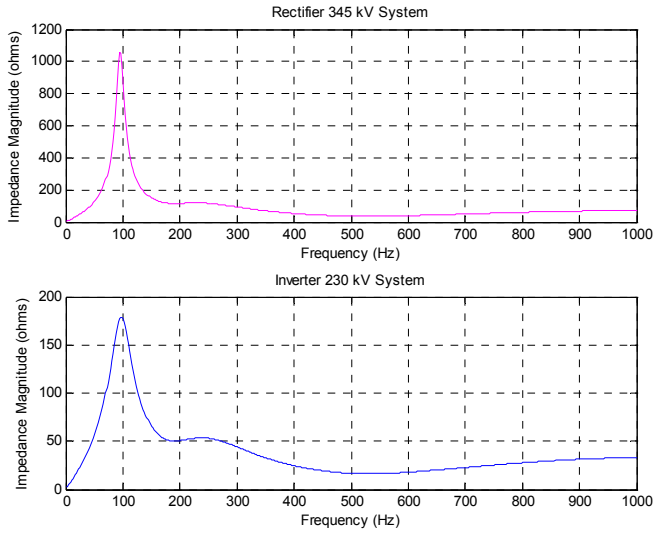

Figure 4-7: *Impedance magnitude characteristic of the AC sides of the benchmark model.*

The CIGRE benchmark model has been implemented in SIMULINK using physical modelling blocks included in SimPowerSystems. The complete model is presented in Figure 4-8.

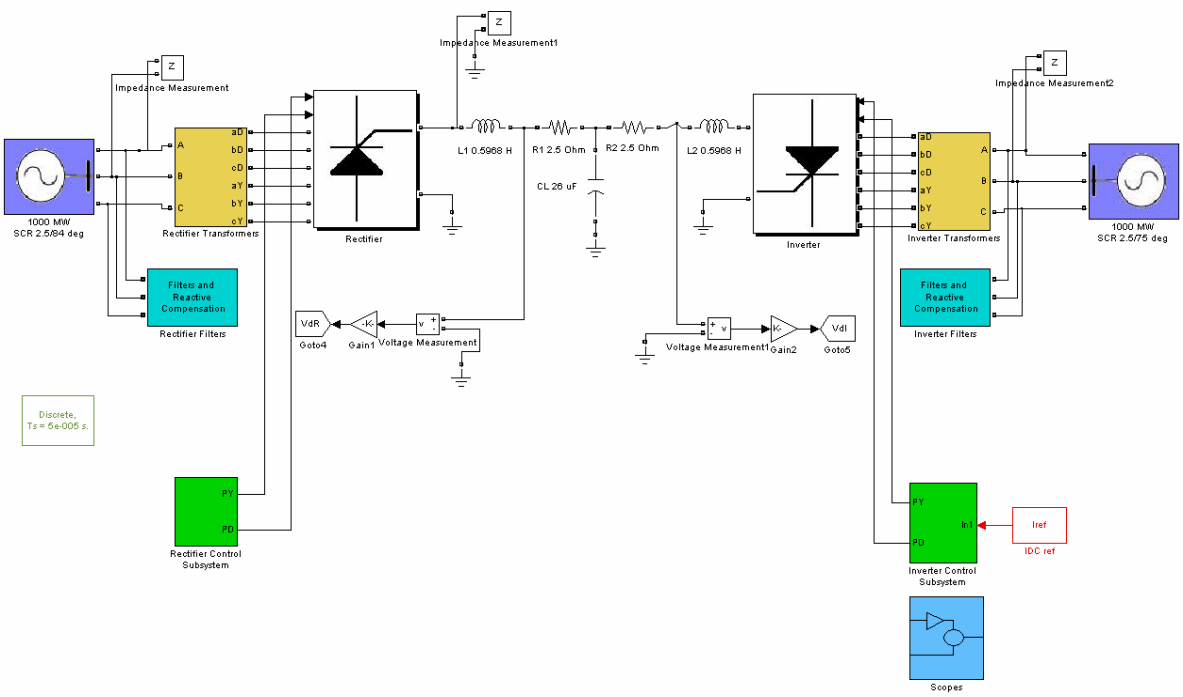

Figure 4-8: *CIGRE benchmark model and its control in SIMULINK.*

Twelve-pulse converters are implemented using the six-pulse basic block available in SimPowerSystems library. Figure 4-9 shows the inverter case.

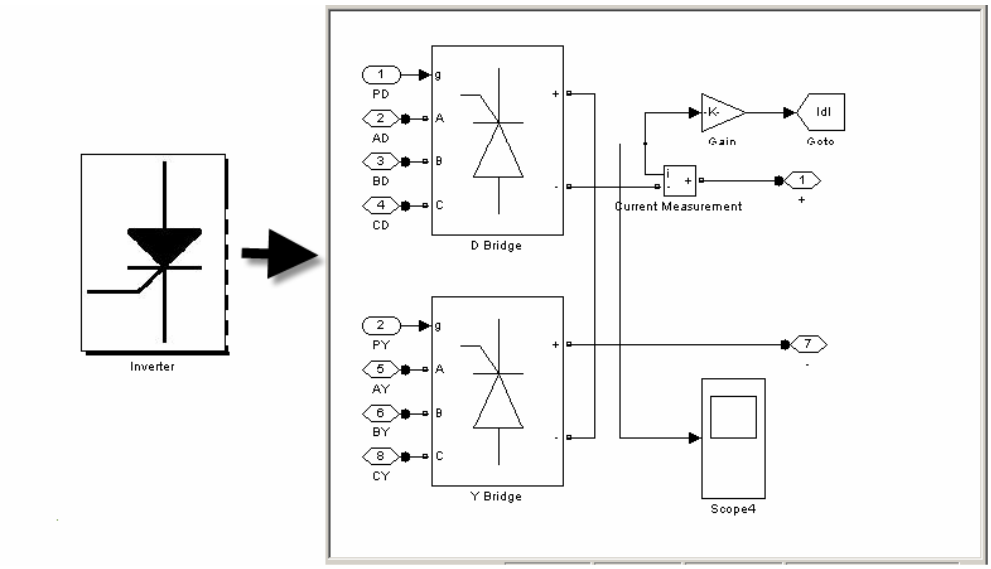

Figure 4-9: *Inverter Block Configuration.*

The equivalent AC system at the rectifier side is termed R-R-L type and is suitable to achieve the same impedance angle for the fundamental and the third harmonic [8]. This equivalent system is modelled using the three phase source block included in SimPowerSystems (see Figure 4-10).

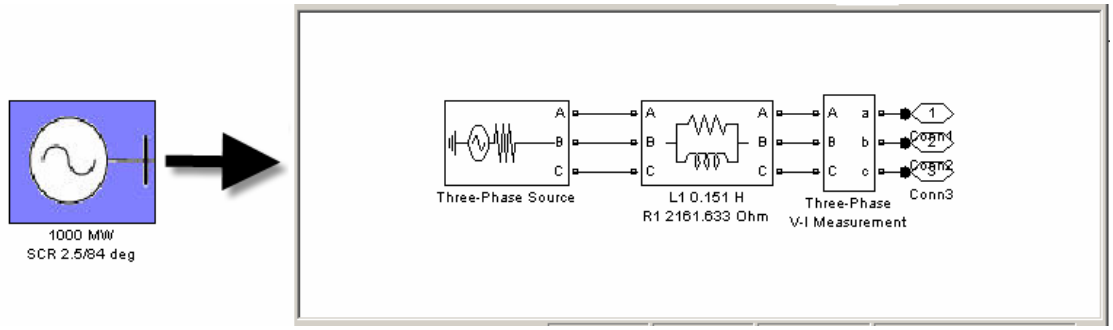

Figure 4-10: *Configuration of the Equivalent AC system at Rectifier Side.*

On the other hand, the equivalent AC system at the inverter side of the CIGRE benchmark model is R-L-L type. Its main characteristic is to exhibit a higher damping for the lower harmonics. Likewise that the other side, the AC system at the inverter uses the three phase source block included in SimPowerSystems. Figure 4-11 shows its configuration.

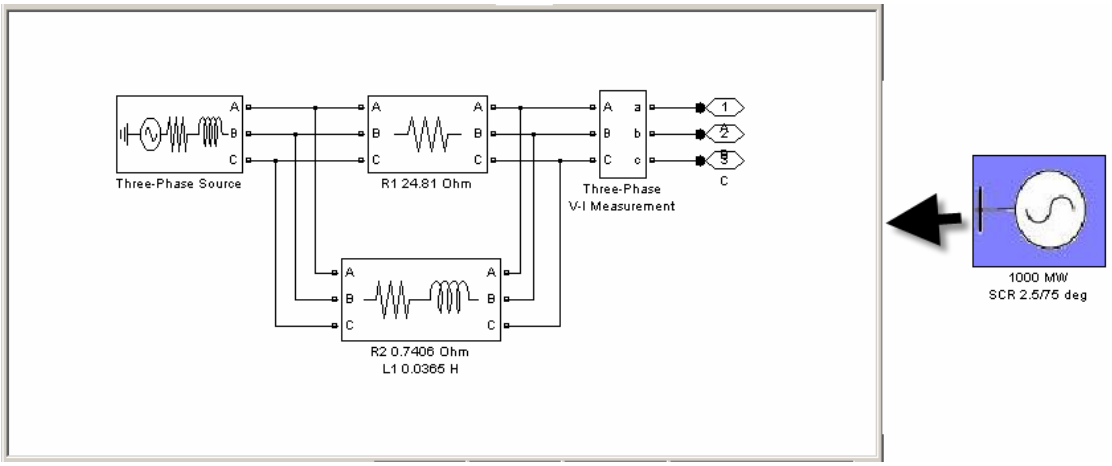

Figure 4-11: *Configuration of the Equivalent AC system at Inverter Side.*

4.5. HVDC Control Scheme

The structure of the control system for the CIGRE benchmark model follows the features described in sections 4.1, 4.2, and 4.3.

A general functional diagram of the control scheme implemented is depicted in Figure 4-12. The control strategy for the CIGRE model is designed to keep constant current (constant current mode CCM) at the rectifier and constant voltage at the inverter (constant extinction angle mode CEAM).

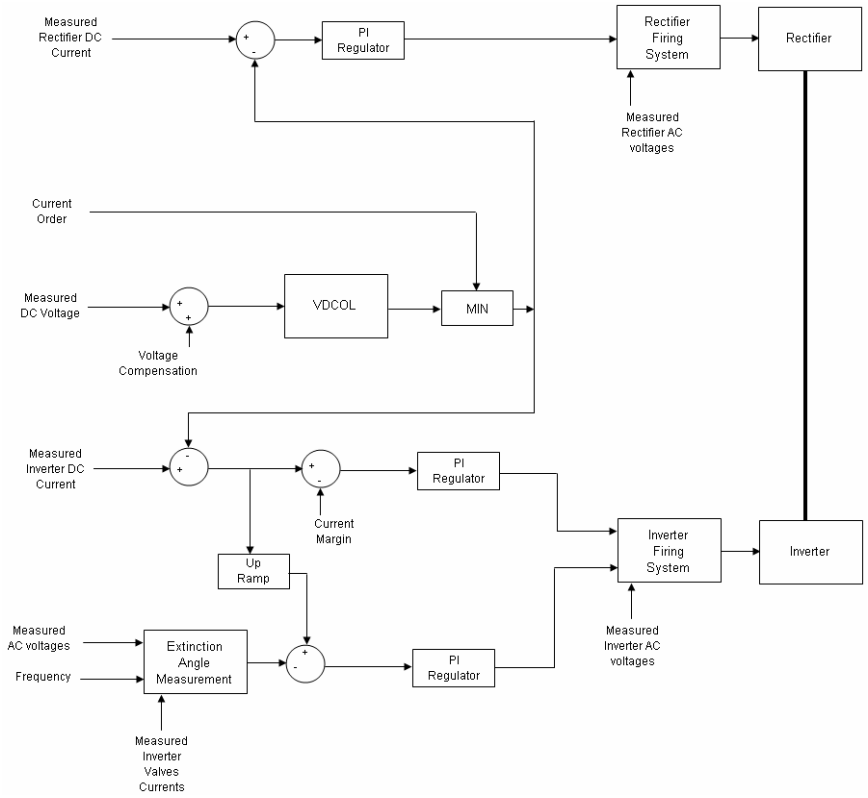

Figure 4-12: *Functional control scheme.*

Generally speaking the control system receives a current order, which indeed decides the active power to be transmitted, and then comparing with the measured DC current determines the firing angle needed at the rectifier. Simultaneously the firing angle at the inverter is determined using the measured DC voltage and current along with the extinction angle at the inverter.

The constant current mode at the rectifier is achieved using a typical PI regulator, which acts according to the error obtained from the measured and the desired current. Gain and time constants for this block have been tuned applying small perturbations to the system. Likewise, a couple of PI regulators dealing with the DC current and the extinction angle are used to control the firing angle at the inverter.

The DC voltage and current static characteristics used to set the voltage dependent current order limiter are sketched in Figure 4-13. As can be observed only

the inverter characteristic considers a VDCOL. This is especially useful when short-time dynamics is studied [8].

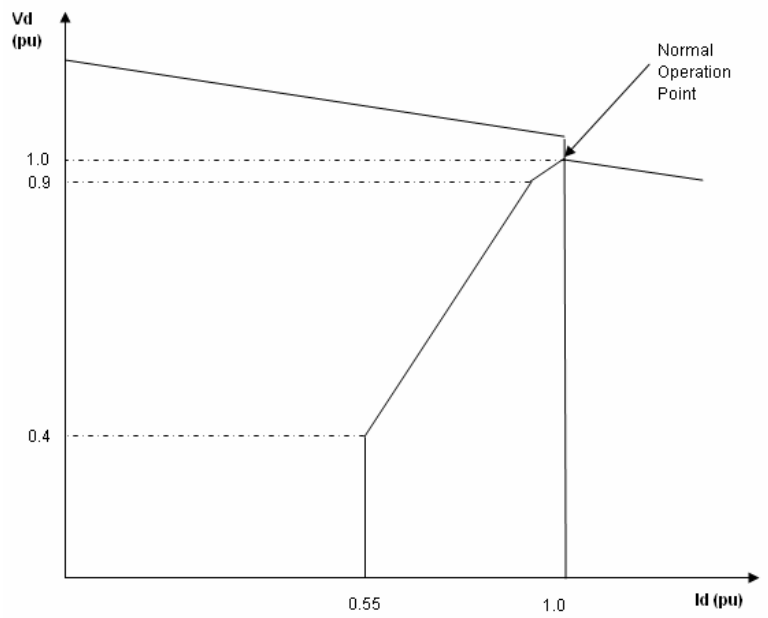

Figure 4-13: *Rectifier and inverter static operating characteristics.*

Each block in the Figure 4-12 has been implemented in SIMULINK. Figure 4-14 depicts the structure of the rectifier control subsystem. The heart of this subsystem is formed by the PI controller and the rectifier firing subsystem. The former shapes the vertical constant current characteristic (see Figure 4-13) and the latter determines the firing pulses required by the converter.

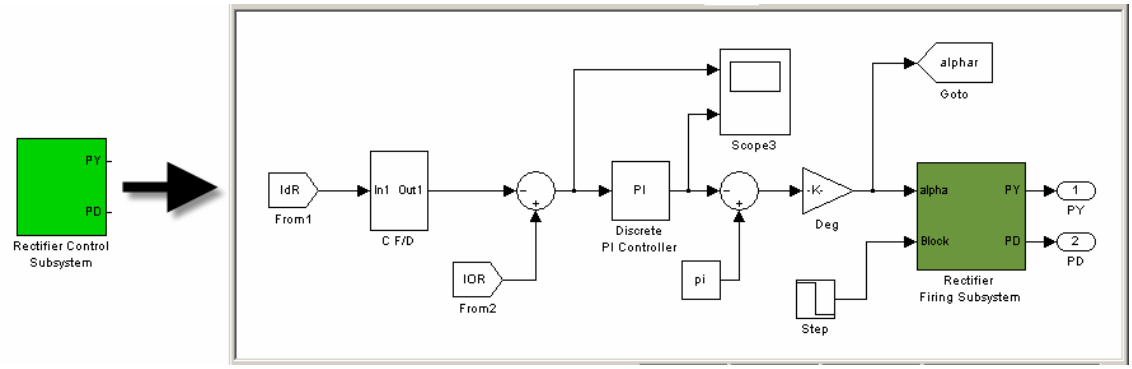

Figure 4-14: *Rectifier Control Subsystem.*

Converter firing control systems are classified mainly in two types. The individual phase control (IPC) and the equidistant pulse control (EPC) [16]. In the case of the individual phase control, the firing pulses are generated individually for each valve considering zero crossing of the commutation voltage. In contrast, in the

equidistant pulse control valves are ignited at identical time intervals. The rectifier firing subsystem used for the CIGRE model is shown in the next figure.

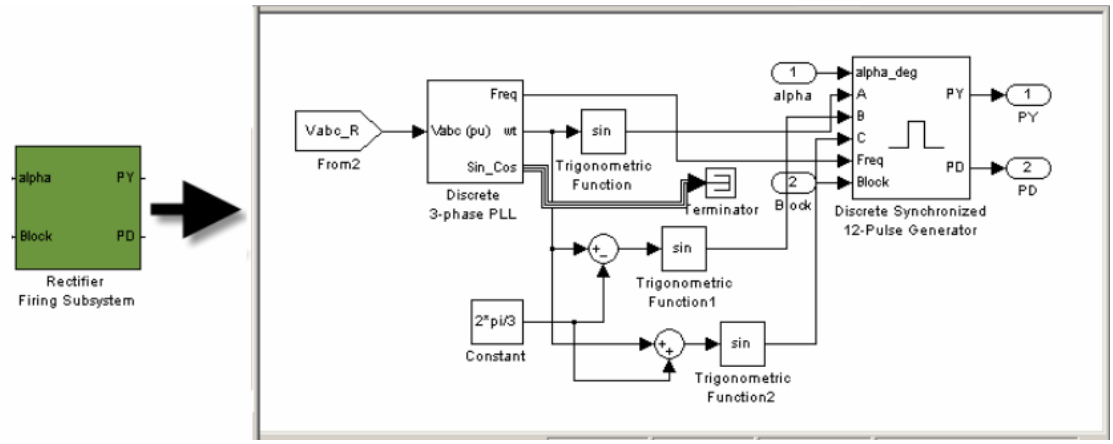

Figure 4-15: *Rectifier Firing Control Subsystem.*

The configuration of the inverter control subsystem is shown in the Figure 4-16. Likewise the rectifier case, this control subsystem mainly consists of PI controllers and a firing system, but additionally it contains the block modelling the VDCOL characteristic.

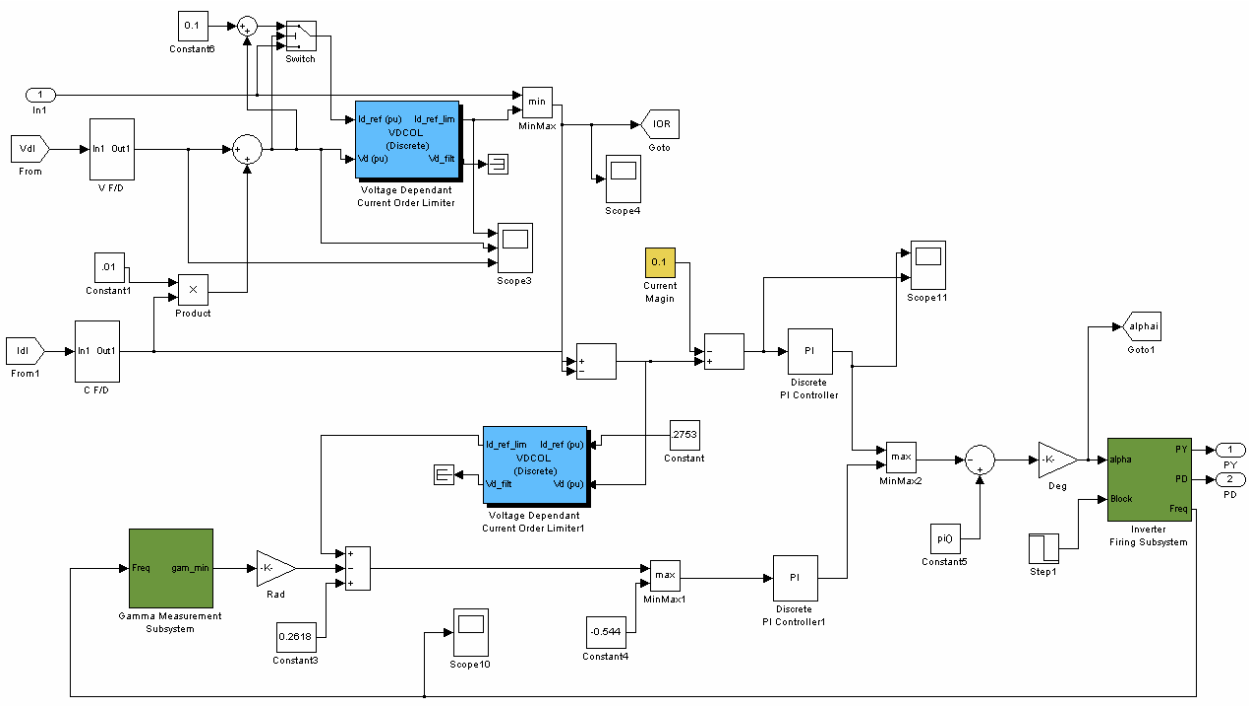

Figure 4-16: *Inverter Control Subsystem.*

Some simulations have been run using the control system described above for the CIGRE-two terminal HVDC system. The DC link is started by fixing a DC current reference (1 pu normally). Runtime is fixed at 2 seconds and the time step is 50 microseconds. Steady state condition is reached in around 0.4 seconds. Responses of the model are shown in the next figures.

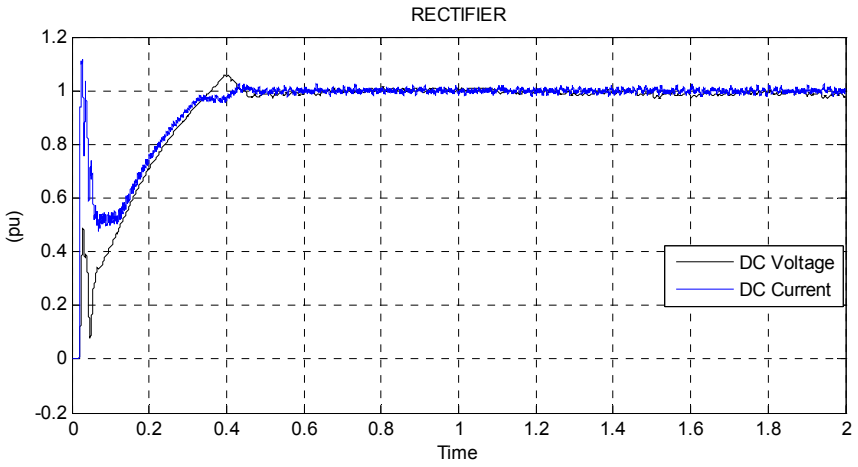

Figure 4-17: *DC Voltage and Current at Rectifier Side Obtained Using SIMULINK.*

Behaviour of both DC current and voltage at the rectifier side are sketched in the Figure 4-17. Same signals are depicted in the Figure 4-18 for the inverter side.

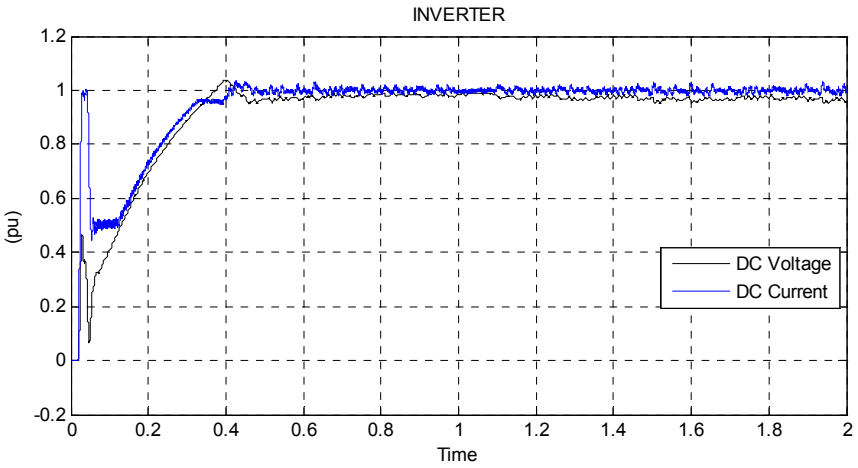

Figure 4-18: *DC Voltage and Current at Inverter Side Obtained Using SIMULINK.*

A three phase to ground fault with duration of five cycles is applied at the inverter side of the system to observe the dynamic response of the control scheme. Fault is started at 0.7 seconds. Results are depicted in Figure 4-19 and Figure 4-20.

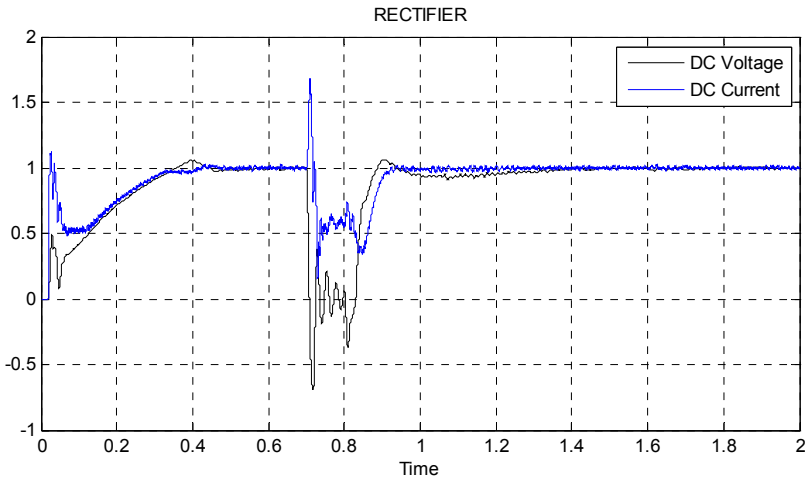

Figure 4-19: *DC voltage and current at rectifier side during a three phase fault at the inverter side obtained using SIMULINK.*

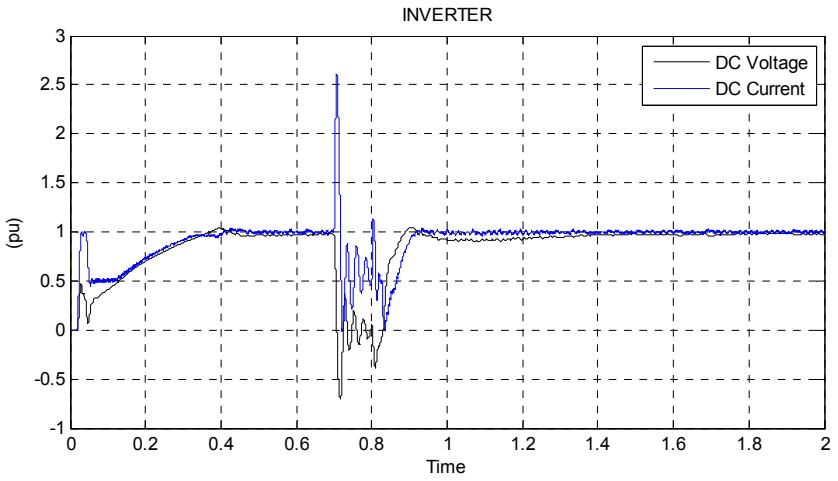

Figure 4-20: *DC voltage and current at inverter side during a three phase fault at the inverter side obtained using SIMULINK.*

The coordinated action of the inverter and rectifier regulators achieves to settle the system back to steady-state. Results show that the time to recover pre-fault conditions is approximately 0.45 seconds.

A fault to ground in the DC link near to the rectifier is additionally simulated. Its duration is set 0.1 seconds, starting at 0.7 seconds. Figure 4-21 and Figure 4-22 show responses obtained using SIMULINK. The sudden increase of the current when the fault appears is followed by the action of the VDCOL, which causes the DC current order to be kept at its minimum value according to the static operating characteristic (Figure 4-13). After the fault is cleared the current is increased to the rated value following the slope of the same curve set in the VDCOL block.

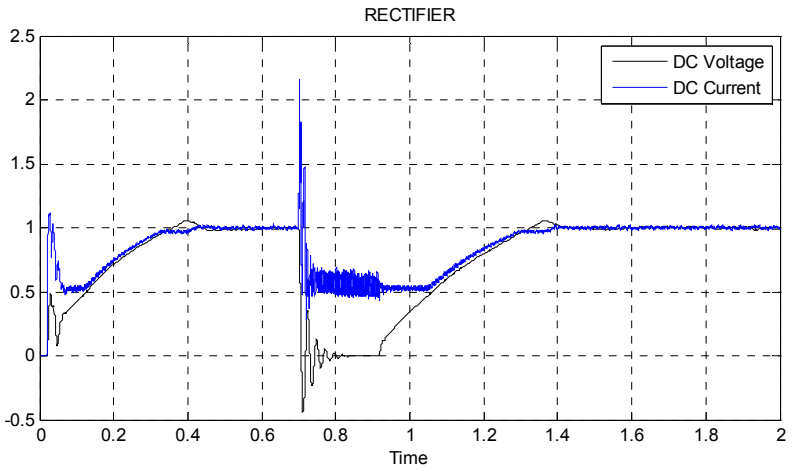

Figure 4-21: *DC voltage and current at rectifier side during a fault in the DC link obtained using SIMULINK.*

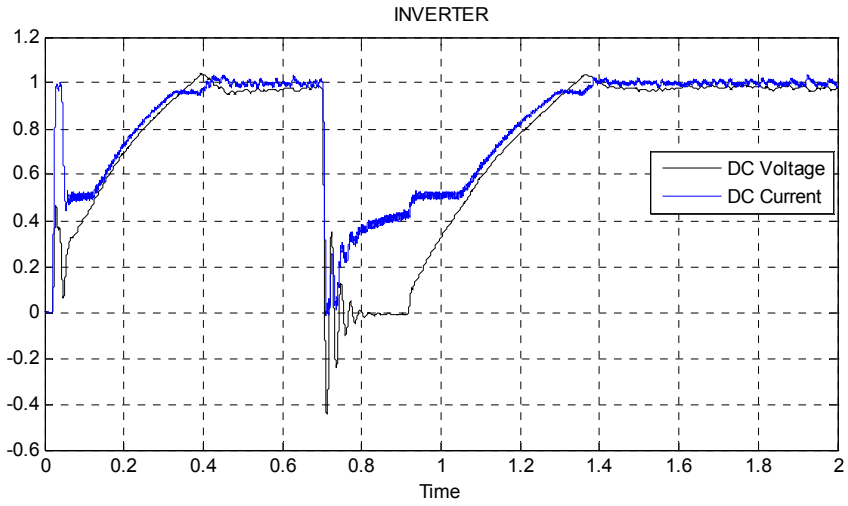

Figure 4-22: *DC voltage and current at inverter side during a fault in the DC link obtained using SIMULINK.*

Firing angles generated by the control system, in the case of a fault in the DC link, are depicted in Figure 4-23. Responses show the incursion of the rectifier firing angle into the inverter region in order to extinguish the fault. Correspondingly the inverter firing angle is forced to its minimum value.

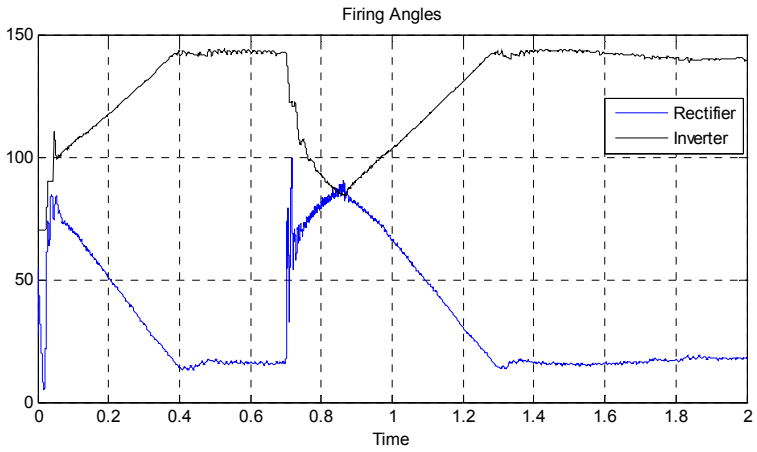

Figure 4-23: *Firing angles applied to converters (DC fault case).*

5. Small Signal Stability Analysis and Control Design

Analysis and control of oscillatory behaviour and dynamic stability in power systems is primordial. Methods based upon properties of dynamic systems are employed to determine oscillatory instabilities and their interactions.

Small signal stability refers to the ability of the power system to keep on synchronism notwithstanding small disturbances always present in the normal operation of the system. In general, instabilities in power systems subject to small disturbances are of two types. Firstly a steady increase in generator rotor angle due to low synchronizing torque and secondly rotor oscillations of increasing amplitude due to lack of damping torque [7]. Nowadays instabilities of the second type are more likely in power systems.

Analysis of small signal stability rests on the fact that being the applied perturbations to the system considerably small, it is then possible to linearise the system around an operation point. In this way complex nonlinearities inherent to all power system are duly left out and thus techniques of analysis of linear dynamic systems can be used. Some details of these methods are exposed in the next sections.

5.1. Space State Representation and Linearization

A general autonomous dynamic system of order n can be represented as a set of first order nonlinear ordinary differential equations:

$$\dot{x} = f(x,u) \tag{5-1}$$

Where the vector column x is termed as the state vector and the vector column u as the vector of inputs of the system. Output variables, which can be observed on the system, may be expressed in terms of state variables (namely, entries of matrix x) and the input variables (entries of matrix u) as:

$$y = g(x,u) \tag{5-2}$$

Being g a vector of nonlinear functions relating state and input variables [7].

Any power system can be represented according to equations (5-1) and (5-2). To achieve this space state representation, each component of the network is expressed as a set of first order ordinary differential equations. Accordingly in general the vector of state variables x of the system is formed by [17]:

- The angular positions and the angular velocities of the rotors of the machines.
- The electromagnetic state variables of the machine.
- The state variables relating to the excitation control systems
- The state variables relating to the speed-governor systems

Alternatively, the vector of inputs u includes voltage-regulator and speed-governor references. In the case of HVDC systems embedded in AC power systems, a special modelling is required in order to fulfil the space state representation. Details of the formulation of HVDC links for use in small signal stability studies are found in [23].

Now if x_0 is an operation point of the system corresponding to a condition of equilibrium being u_0 its input vector, then according to equation (5-1), the following can be stated:

$$\dot{x}_0 = f(x_0, u_0) = 0 \tag{5-3}$$

Using Hartman-Grobman theorem [24], it is possible to linearise the dynamic system around the operation point. Therefore in a small neighbourhood of x_0 the nonlinear dynamical system (5-1) with outputs (5-2) is qualitatively similar to the linear system:

$$\begin{aligned} \dot{x} &= Df(x_0)x + Df(u_0)u = Ax + Bu \\ y &= Dg(x_0)x + Dg(u_0)u = Cx + Du \end{aligned} \tag{5-4}$$

State vector x has dimension n for a system of order n and hence A (the state matrix) has dimension of nxn. If the order of the input vector and the output vector are r and m respectively, then B (or control matrix) has dimension nxr, C (the output matrix) has dimension mxn, and D (the feed-forward matrix) has dimension mxr.

Standard theory of linear dynamical systems can be applied to the system (5-4) and conclusions about stability and other properties can be found. In particular, important outcomes are derived from eigenvalues and eigenvectors of the state matrix.

Eigenvalues of state matrix A are defined as the scalar parameters λ for which the next equation has non-trivial solution:

$$A\Phi = \lambda\Phi \tag{5-5}$$

Where Φ is an nx1 vector. In other terms, non-trivial solution of equation (5-5) is possible under the next condition:

$$\det(A - \lambda I) = 0 \tag{5-6}$$

Expression (5-6) which is called characteristic equation represents an n-degree polynomial and its n roots correspond to the eigenvalues of the state matrix A. For each eigenvalue λ_i of the state matrix A, there is a vector Φ_i, which satisfies the equation (5-5). Such a vector is called the eigenvector associated to the eigenvalue λ_i. Besides, if the eigenvector satisfies the form of the equation (5-5) is referred to as right eigenvector, in opposition to that which satisfies the other also possible expression (5-7).

$$\Psi A = \lambda\Psi \tag{5-7}$$

Each nx1-vector Ψ_i in the last expression is named the left eigenvector of A associated to the eigenvalue λ_i. Right and left eigenvectors of A also satisfy:

$$\begin{aligned} \Psi_j\Phi_i &= 0 \\ \Psi_j\Phi_j &= k_j \end{aligned} \tag{5-8}$$

Denoting i and j the i-th and j-th eigenvalue of the state matrix A and k_i a constant different of zero.

A useful transformation is obtained from system (5-4) using the following definitions:

$$\begin{aligned} x &= \Theta z \\ \Theta &= \left[\Phi_1\ \Phi_2 \cdots \Phi_n\right] \\ \Omega &= \left[\Psi^T{}_1\ \Psi^T{}_2 \cdots \Psi^T{}_n\right]^T \\ \Lambda &= \begin{bmatrix} \lambda_1 & 0 & \cdots & 0 \\ 0 & \lambda_2 & \cdots & 0 \\ 0 & 0 & \ddots & 0 \\ 0 & 0 & \cdots & \lambda_n \end{bmatrix} \end{aligned} \tag{5-9}$$

Where z corresponds to a new state vector. Hence dynamic system (5-4) can be expressed in terms of the new state vector as:

$$\dot{z} = \Lambda z + \Theta^{-1} B u = \Lambda z + B' u$$
$$y = C\Theta z + Du = C' z + Du \qquad (5\text{-}10)$$

Dynamic system in the form of (5-10) is termed decoupled. Being Λ a diagonal matrix (see (5-9)) is clear that each transformed state variable z_i is associated with only one dynamic mode corresponding to the eigenvalue λ_i. Entries of matrix B' determine the controllability of the different modes while entries of the matrix C' determine their observability [7]. Others features as sensitivities and participations can also be derived from eigenvectors and eigenvalues analysis [19].

An interesting and useful representation of the system (5-10) can be obtained using Laplace transform. In this way a transfer function in terms of eigenvalues and eigenvectors of the state matrix is found. If it is assumed that in (5-10) the output vector is independent of the input vector, namely $D=0$, then the transfer function of the system is given by:

$$G(s) = \frac{y(s)}{u(s)} = C\Theta\left(sI - \Lambda\right)^{-1}\Omega B \qquad (5\text{-}11)$$

Since Λ is a diagonal matrix, then the transfer function can also be stated as:

$$G(s) = \sum_{i=1}^{n} \frac{R_i}{s - \lambda_i}$$
$$R_i = C\Phi_i \Psi_i B \qquad (5\text{-}12)$$

Terms R_i are called the residues and are obtained using eigenvector of state matrix A. Poles of the transfer function G(s), according to expression (5-12), correspond to the eigenvalues of the matrix A.

In the specific case of (5-4) representing an electric power systems, consisting of n machines, the eigenvalues λ_i of the state matrix A supply information regarding stability of the system for small variations [17]. In particular, the characteristics of the $n\text{-}1$ electromechanical oscillation modes can be obtained from the associated pairs of eigenvalues written in the form:

$$\lambda_{h(1,2)} = -\zeta_h \omega_{nh} \pm j\omega_{nh}\sqrt{1-\zeta_h^{\,2}} = \sigma_h \pm j\omega_h \qquad (5\text{-}13)$$

Identification of the eigenvalues λ_h among all the λ_i is achieved using the eigenvector of the state matrix A by looking for those whose elements have a relatively large module corresponding with the electromechanical state variables (angles and angular velocities). Nonetheless, it is frequent for this identification to

consider the low values of the dampings for the modes corresponding to the electromechanical oscillations [17].

5.2. Improvement of Damping

One of the main objectives of this work is related to mitigation of electromechanical oscillation modes. For this reason it is pertinent to discuss some theoretical methods directed to achieve that mitigation.

It is a common practice in power systems having electromechanical modes with negative or low damping (lower that 0.03) to add local feedbacks into the excitation controls of suitable chosen generators in order to improve damping [17], [7]. Mentioned feedbacks are generally connected to the speed loops of the generators and their derivatives. Even though the selection of the appropriate generators to apply compensation is an important problem, that will not be treated here. Some procedures regarding this issue can be found in [18] and [22]. Next sections will focus on the design process of the compensation loops described above.

The purpose of the compensation is to shift the eigenvalues corresponding to the critical modes to a new location characterized by a higher damping coefficient. In practice a small shift is enough, for instance a $\Delta\zeta$ of around 0.15 is widely accepted as a safety margin for operation of power systems [26], [17]. In relation to the gain of the additional feedback or compensation, it should be not excessively high to avoid disturbances in voltage regulation mainly. Pole placement technique can be used for the design of the compensator under considerations stated above [25].

Referring to Figure 5-1, *G(s)* represents the transfer function of a system with input *u(s)* and output *y(s)*.

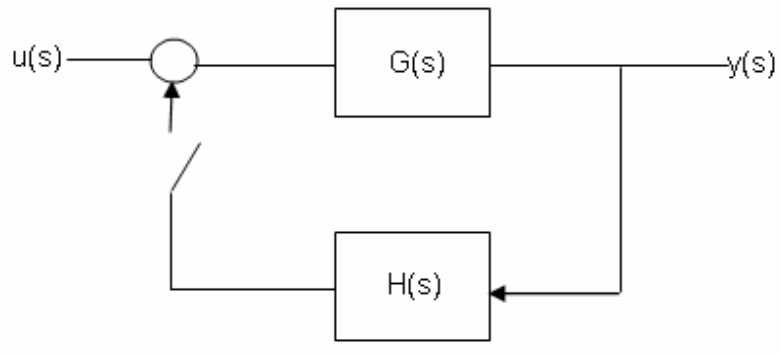

Figure 5-1: *Compensator With Small Gain.*

A close loop with small gain $H(s)$ is added between the two signals. If all the zeros and poles of $G(s)$ and $H(s)$ are distinct, then in the neighbourhood of any pole λ_i (see equation (5-12)) the transfer function can be written as:

$$G(s) \approx \frac{R_i}{s - \lambda_i} \tag{5-14}$$

Hence, regarding the system depicted in Figure 5-1 (closed feedback loop), the complete transfer function is given by [17]:

$$y(s) = \frac{G(s)}{1 - G(s)H(s)} u(s) \approx \frac{R_i}{s - (\lambda_i + H(\lambda_i)R_i)} u(s) \tag{5-15}$$

In view of that, closing the compensation loop causes a shift in the pole λ_i, which according to equation (5-15) is given by:

$$\Delta\lambda_i = H(\lambda_i)R_i \tag{5-16}$$

Thus the shift of the pole λ_i depends on the transfer function of the compensation block calculated at the eigenvalue and its residue (eq. (5-12)). As is expected the same approximation (5-15) can be applied to those poles λ_h associated with the electromechanical oscillations with reduced damping. Given any of these electromechanical modes λ_h is clear from (5-16) that:

$$\left|\Delta\lambda_h\right| = \left|H(\lambda_h)\right|\left|R_h\right| \tag{5-17}$$

This means that at all points of the circumference, with centre at λ_h and whose radius is $|\Delta\lambda_h|$, correspond the same gain [17]. For a given value of $|H(\lambda_h)|$, among all the possible shifts $\Delta\lambda_h$, the one to which the maximum damping increase is achieved is the shift in the direction $j\lambda_h$, that is with ω_{nh} constant.

Equation (5-17) also indicates that the compensation is more effective if the chosen input has a high residue R_h, therefore it is desirable to pick up an input with the highest observability possible [18]. The shift of the selected eigenvalue can be done by shaping the phase of $H(s)$ using phase lead compensation. Practical compensators of this type have the general form shown in the next expression [20]:

$$H(s) = \left[\frac{1 + a_i\tau_i s}{1 + \tau_i s}\right]^m \tag{5-18}$$

Being τ_i the time constants and m the number of lead-lag pairs (m is between 1 and 4 in common applications).

The feedback transfer function must compensate the phase lag of R_h on the frequency of the corresponding electromechanical mode λ_h (see Figure 5-2).

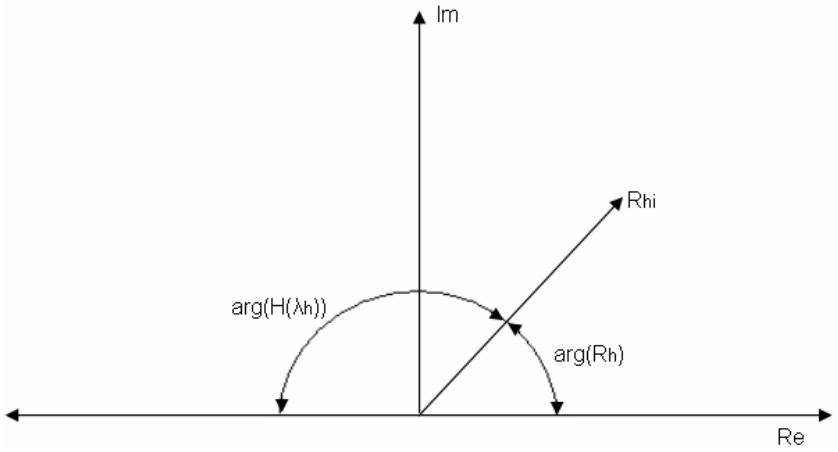

Figure 5-2: *Effect of Residue Compensation [20].*

The desired compensation of the *h*-th mode (Figure 5-2) can be derived by the sequential tuning of the *i*-th transfer function according to [20]:

$$\varphi_i = \frac{\pi - \arg\{R_{hi}\}}{m}$$
$$a_i = \frac{1+\sin\varphi_i}{1-\sin\varphi_i} \qquad (5\text{-}19)$$
$$\tau_i = \frac{1}{\omega_h\sqrt{a_i}}$$

Due to practical reasons the maximum phase lead of a feasible compensator, indicated by φ_i in the equation (5-19), must be smaller than 1 radian. In a multi-machine power system, the phase lag of the argument of the residue R_h may vary from few degrees to more than 180 degrees [20]. Consequently, compensator (5-18) will require a sequential tuning using (5-19) in order to improve damping.

It is common practice to add a washout block to the compensator to filter DC signals. Washout time constant (T) is usually chosen between 5 and 10 seconds [18], [21]. Thus $H(s)$ becomes:

$$H(s) = \frac{sT}{1+sT}\left[\frac{1+a_i\tau_i s}{1+\tau_i s}\right]^m \qquad (5\text{-}20)$$

Procedure described can be used to design power systems stabilizers (PSS) (see [17], [18], [19], [20], [22]) in order to increase damping and likewise it will be used here to design supplementary controls for HVDC transmission link with the same purpose of damping improvement.

6. Inter-Area Oscillations and Study System

6.1. Inter-Area Oscillations

Electromechanical oscillations between interconnected synchronous generators are proper of power systems. Alternating current generators remain in synchronism because of the self-regulating properties of their interconnection, however due to the control systems on generators these properties associated mainly to the natural system damping can be undermined leading to instability [26], [28]. This type of instability is characterized by the emerging of oscillation modes of increasing amplitude.

Commonly, in tightly interconnected systems, the frequency of electromechanical swing modes range from 1 Hz to 2 Hz and are usually well damped. These oscillations, named local oscillations, generally are associated with a single generator [27]. However, when large systems are connected by long, relatively weak inter-ties, lower frequency swing modes also result. The response of generator controls to the synchronizing swings associated with these low frequency modes produces a negative damping effect, cancelling accordingly the natural damping of the system. Under these conditions the constantly small changes which the system is normally subjected would give rise to oscillations of increasing amplitude [28]. The main characteristics of these types of oscillations, called inter-area oscillations, are that group of generators are involved and their range frequency is 0.1 Hz to 0.8 Hz.

Inter-area oscillations can strongly restrict power system operations by requiring the curtailment of electric power transfers as an operational measure. These oscillations can also lead to widespread system disturbances if cascading outages of transmission lines occur due to oscillatory power swings [30]. Many instances of unstable oscillations involving inter-area modes in large power systems have been reported and studied [14], [27], [28] and [29]. All these aspects reflect the importance of understanding inter-area phenomenon and its mitigation.

6.2. Base Study System

With the purpose of studying the implications, specially in inter-area oscillations mitigation, of HVDC supplementary control systems embedded in AC power systems, an special and widely studied system is selected. The system has been designed seeking to remark the inter-area and local oscillation phenomena [27]. Being both sufficiently simple to clear the fundamental features of oscillations and besides quite real in terms of system parameters and structure, the model is particularly useful for parameter studies.

The base system is symmetric (see Figure 6-1); it consists of two identical areas connected through a relatively weak tie. Each area includes two generators with identical power outputs and excitation control systems [27]. The symmetrical condition of the model permits to reveal the factors affecting the oscillatory interaction between the two areas.

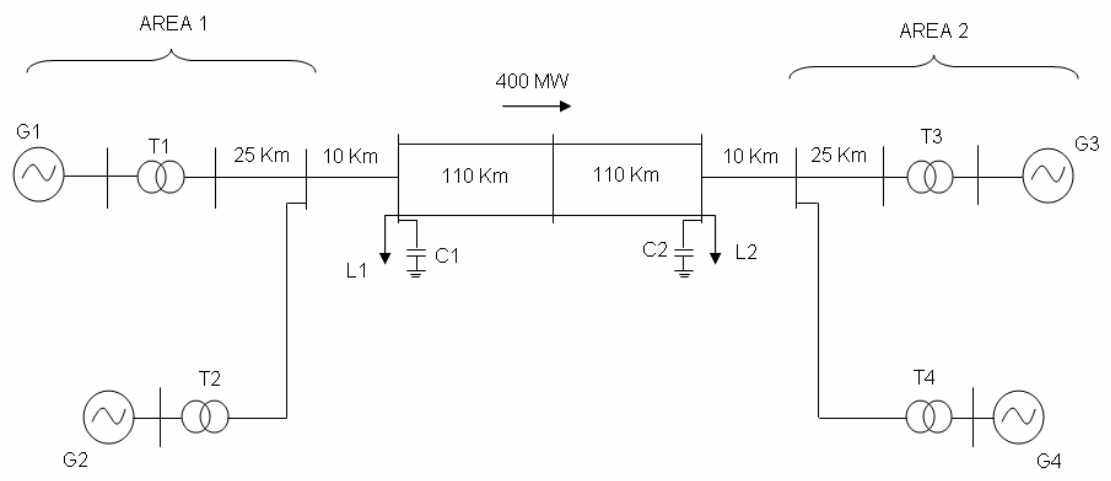

Figure 6-1: *Two Area System [7].*

The rating power and voltage of each generator is 900 MVA and 20 kV respectively. The transmission system nominal voltage is 230 kV and each area has some shunt capacitors added with the purpose of maintaining the voltage profile of the system. Step-up transformers, with unitary off-nominal ratio and 900 MVA of rating power, are used to reach transmission voltage levels.

In the base case, the system is operating with area 1 exporting 400 MW to area 2. Different power flows can be set adjusting the load conditions at each area.

Next table summarizes the main parameters of the system.

Table 1 Two Are System Parameters

ELEMENT	PARAMETERS IN PER UNIT
Generators G1, G2, G3, G4 Sbase = 900 MVA Vbase = 20 kV	X_d=1.8 X'_d=0.3 X''_d= X''_q=0.25 X_q=1.7 X'_q=0.55 X_l=0.2 R_a=0.0025 T'_{d0}=8 s T''_{d0}=0.03 s T'_{q0}=0.4 s T''_{q0}=0.05 s A_{sat}=0.015 B_{sat}=9.6 H=6.5 for G1 and G2 H=6.175 for G3 and G4
Step-up Transformers T1, T2, T3, T4 Sbase = 900 MVA Vbase = 20/230 kV Off-nominal ratio = 1	x_T=j0.15
Transmission Lines Sbase = 100 MVA Vbase = 230 kV	r=0.0001 pu/Km x_l=0.001 pu/Km b_c=0.00175 pu/Km
Loads Sbase = 100 MVA Vbase = 230 kV	P_{L1}=9.67 Q_{L1}=1 P_{L2}=17.67 Q_{L2}=1
Shunt Capacitors Sbase = 100 MVA Vbase = 230 kV	Q_{C1}=2 Q_{C2}=3.5

System of Figure 6-1 presents three electromechanical oscillation modes. Two of them correspond to local inter-plant modes and one remaining corresponding to a low frequency inter-area mode, in which generating machines in one area oscillate against those in the other area [27]. The frequencies of the local inter-plant oscillations depend on the moments of inertia of the generator rotors and additionally on the strength of the system (see section 3). Their values for system in Figure 6-1 are in the range of 0.7 to 1.2 Hz for different operating conditions. In contrast, inter-area modes have frequencies in the range 0.3 Hz to 0.6 Hz [26].

6.3. Study System with HVDC Inter-Tie

The small power system presented in Figure 6-1 has been used in this work adding an HVDC transmission link between the two areas. The complete network modelled and studied is shown in the next figure.

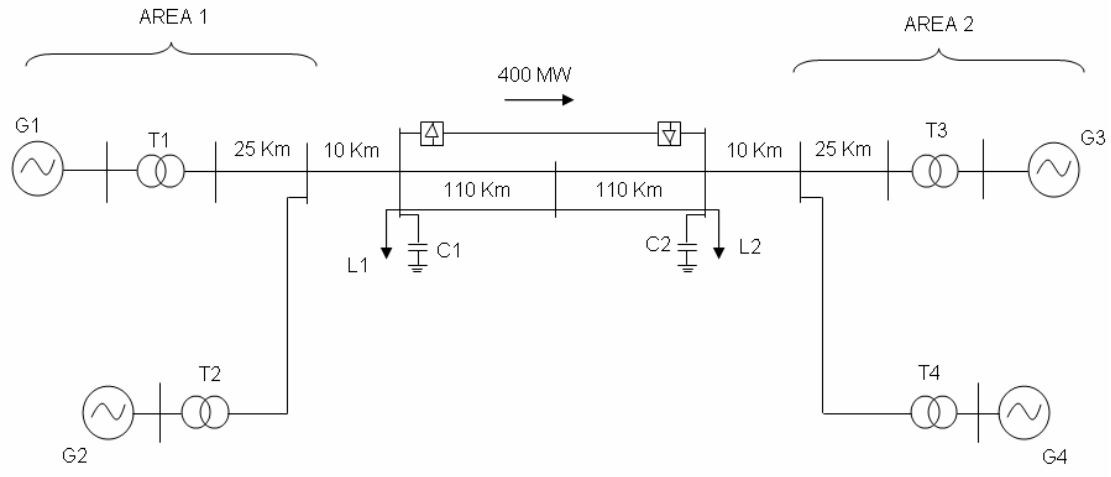

Figure 6-2: *Two Area System with a DC inter-tie [7].*

Parameters of the DC inter-tie are assumed the same of those used in [7]. The HVDC link is represented by a 200 MW monopolar link with rating voltage of 56 kV and a current rating of 3.6 kA. The DC line resistance is 1.5Ω and its inductance 100 mH.

Each converter is formed using two six-pulse bridges (see section 2.2), with associated commutating reactance (X_c) of 0.57Ω, and two converter transformers. According to data given above, the converter transformer can be specified as:

$$Z_{base} = \frac{V^2_{rated}}{S_{rated}} = \frac{(56kV)^2}{200MW} = 15.6\Omega$$

$$Z_{pu} = \frac{X_c}{Z_{base}} = \frac{0.57\Omega}{15.6\Omega} = 0.037$$

$$V_2 = \frac{\pi V_{rated}}{3\sqrt{2}N_{BR}} \frac{1}{\cos\alpha_N - \frac{X_c}{2}} = 22.2kV \qquad (6\text{-}1)$$

$$I_2 = \sqrt{\frac{2}{3}} I_{rated} = \sqrt{\frac{2}{3}} 3600 = 2940A$$

$$S = \sqrt{3} V_2 I_2 = 65MVA$$

Where N_{BR} represents the number of six-pulse bridges and α_N the operating firing angle, which is assumed in 18 degrees.

Furthermore, reactive power compensation is added at each side of the DC link using a capacitor bank with rated power of 125 MVAr.

6.3.1. Control Scheme of the HVDC Inter-Tie

The structure of control implemented for the HVDC link of the Figure 6-2 is similar to that described in section 4.5. Figure 6-3 depicts the control scheme used for each converter of the DC inter-tie [31].

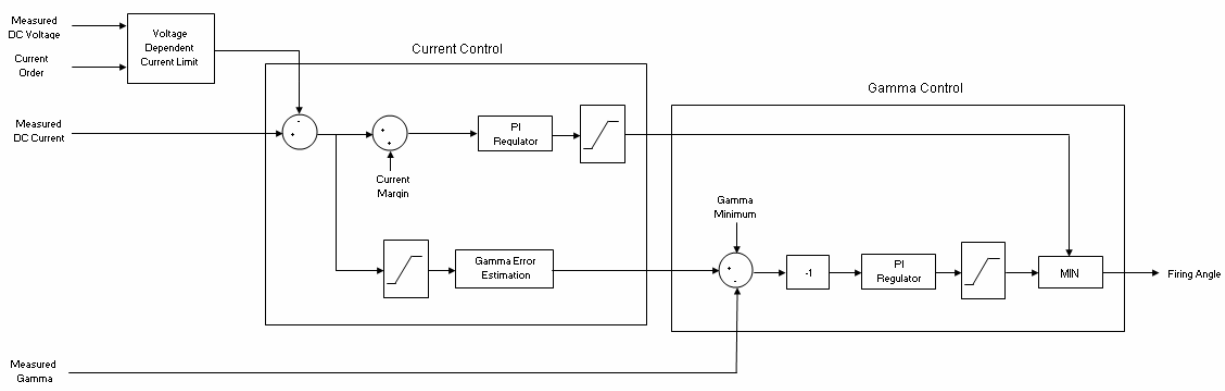

Figure 6-3: *Block Diagram of Converter Controller.*

The voltage dependent current order limiter (see section 4.3) is set according to the characteristic show in Figure 6-4.

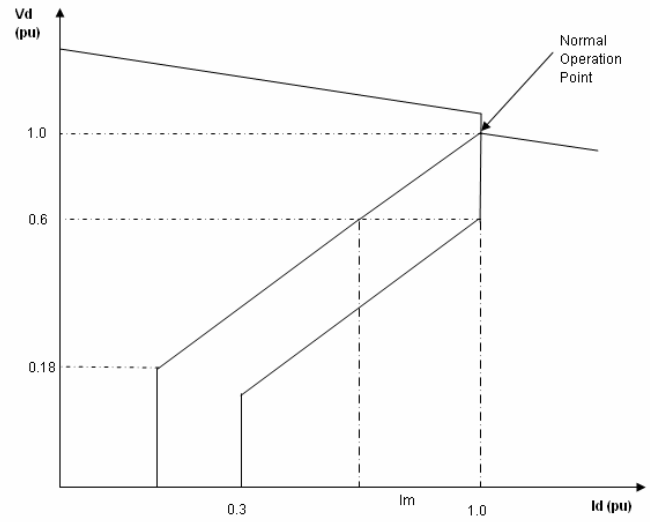

Figure 6-4: *Voltage Dependent Current Order Limits Used in the Converter Control Scheme.*

The current margin is adjusted to 10% of the rated current. The effect of the current margin is to modify the current order so that each converter attempts to control DC current to a different level than the other. If under normal operating conditions the converter is not controlling current, then it is forced into establishing DC voltage by setting the current margin positive for an inverter. One converter in the two terminals DC link configuration determines voltage in this way. The remaining converter (rectifier) is set in current control with zero current margin. This forces the desired firing angle at the inverter to the maximum level allowed, with the result that the gamma control in the valve group controller takes over the firing angle order. A gamma equal to the minimum gamma order setting is what the inverter attempts to produce. With the gamma controller active, the inverter is no longer in current control. In this way the same block diagram shown in Figure 6-3 can be used to control both sides of the HVDC link.

The inputs of the converter controller are the measured DC current, the measured DC voltage, the measured extinction angle, and the current order. Both measured DC current and DC voltage are filtered considering transducers effects. Transducers usually have a response time ranging between 0.5 ms to 50 ms [1]. Once signals are acquired and limited by the voltage dependent current order limit, the next step is to produce an alpha order from a proportional-integral controller, acting from the error between current order (CO) and measured current (CD). This is performed by the current controller indicated in the Figure 6-3. Next step in the controller is the gamma controller. This block, active only for inverter mode, selects the actual firing angle. If the firing angle order from the current controller increases to the point where the corresponding extinction angle becomes less than the desired gamma then the gamma regulator will determine the firing angle.

From an operating point of view it is convenient to control DC power rather than DC current through the HVDC inter-tie [2]. This can be achieved implementing a master power control, which uses a DC power order and the measured DC voltage as inputs (Figure 6-5). Once the DC voltage is measured, the signal is filtered setting the time constant T1. In the case of low short circuit ratios this time constant must be greater than one second to attain stability in the HVDC link. Furthermore, a minimum DC voltage is set in order to avoid undesirable over currents.

Fast response in the HVDC inter-tie is maintained adjusting the time constant T2 in the lag block (see Figure 6-5) ranging from 5 ms to 50 ms. After this some limits in the output current are established and then current orders are sent to each converter control.

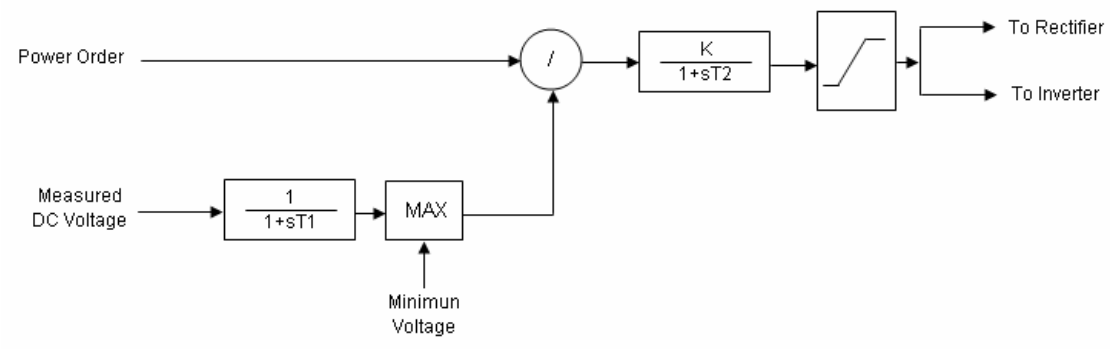

Figure 6-5: *Master Power Control.*

6.4. Generators and Excitation Type

Generators in the system of Figure 6-2 are represented using a generalised machine model. Figure 6-6 shows how this representation of a synchronous generator is referred to dq axis [32].

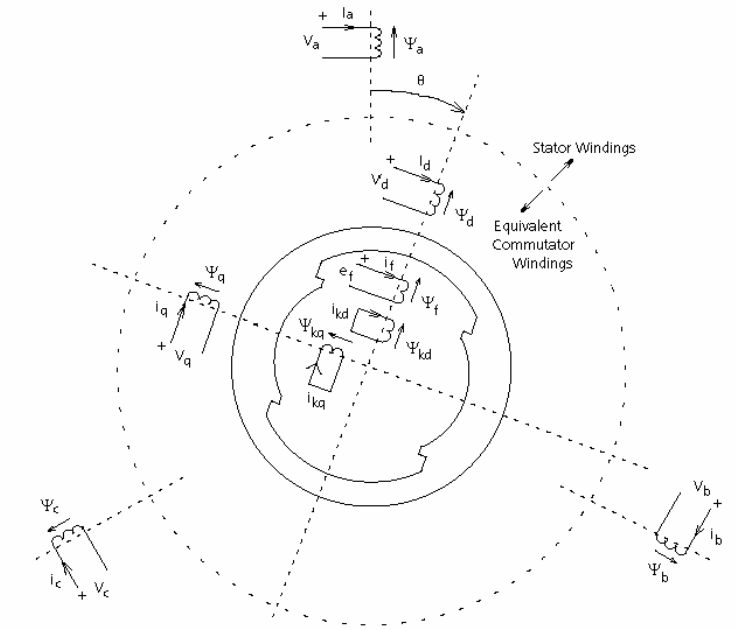

Figure 6-6: *Synchronous Generator Representation [32].*

Considering that some previous results have shown that a detailed representation of the generators along with fast excitation systems are the most suitable to study oscillatory behaviour of networks [27], a detailed model of the machines, based on representation described above, have been used in this work and their excitation systems have been chosen of the fast type.

The configuration of the fast excitation system used in this work is illustrated in the next figure.

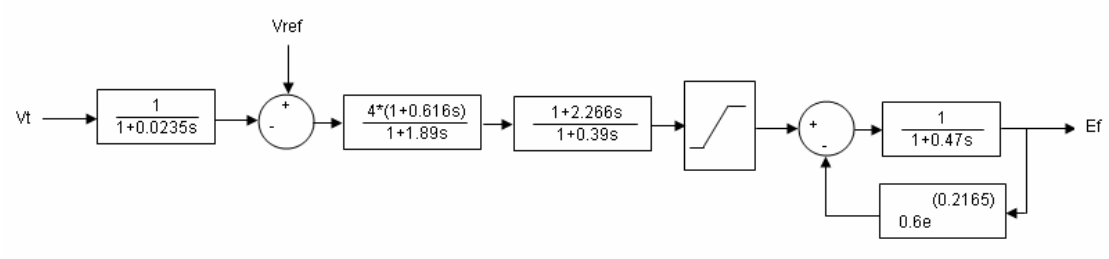

Figure 6-7: *Fast Exciter Used in the Study System.*

This static exciter considers saturation and its response is sufficiently fast to fulfil the requirements stated before.

In addition to the voltage regulation control of Figure 6-7 a power system stabilizer (PSS) is added to the generators of the study system described before[1]. The main function of the power system stabilizers is to increase the damping of the generator rotor oscillations. To achieve this damping improvement the stabilizer is designed to produce a component of electrical torque in phase with the rotor speed deviations [7]. The configuration of the power system stabilizer used modelling the study system is depicted in the Figure 6-8.

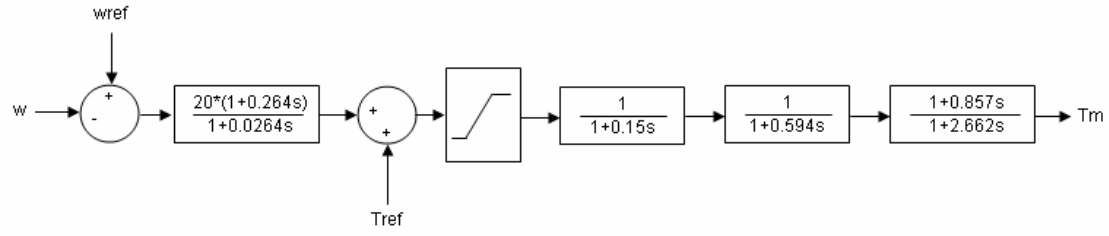

Figure 6-8: *PSS Used in the Study System.*

[1] The power system stabilizer has been designed and tuned along with Professor Kumar Venayagamoothy, who is the director of the real time power and intelligent system laboratory at University of Missouri Rolla.

7. PSCAD/EMTDC modelling

The two area power system described in the foregoing section has been implemented using PSCAD/EMTDC.

PSCAD is a powerful and flexible graphical user interface to the world-renowned EMTDC solution engine [32]. Typical PSCAD/EMTDC applications include control system design and coordination of FACTS and HVDC and optimal design of controller parameters among many others. This platform supports linear and nonlinear systems modelled in continuous time, sampled time, or a hybrid of the two.

Several basic components of electrical networks can be found already modelled in the extensive library supported by PSCAD/EMTDC. A brief description of those components used in this work is given in the next sections.

7.1. Generators

PSCAD/EMTDC contains a detailed component modelling main characteristics of a synchronous machine. This model follows the representation presented in the Figure 6-6 and permits to adjust all the parameters for the generators according to those detailed in section 6.2. Additionally, the component includes an advance method to initialize and start-up the machine. The general sequence of this process is as following [32]. At time=0, machine is a fixed source at its terminals whose voltage magnitude and phase is as entered by the user which might correspond to the values obtained from a load flow program solution of the network. The network solution progresses from the start-up with the voltage source firmly fixed so that the network can reach its steady state condition. To ensure that the steady state condition of the network is reached smoothly the source voltage magnitude may ramp to its specified value over a time interval entered by the user. When the steady state of the network has been reached, the user may choose to switch the voltage sources representing each machine to a constant speed condition with the machine model in place. The machine equations will hold. However, the mechanical dynamics will not be in place during this period and the rotor will be spinning at a constant speed corresponding to the base angular frequency specified by the user. At the time of transition from source to machine model, exciter and stabilizer models (if used with the machine model) can be conditioned to give an 'initialized' output so that the transition from

source to machine is seamless. The exciter and stabilizer models are initialized during the period the machine is acting as a source. Information for initialization can be fed to these models (terminal voltage, current etc.) from the machine model. Then machines are unlocked and the system will run free and stable.

Figure 7-1 illustrates the complete model of one generator with its controls implemented in PSCAD/EMTDC.

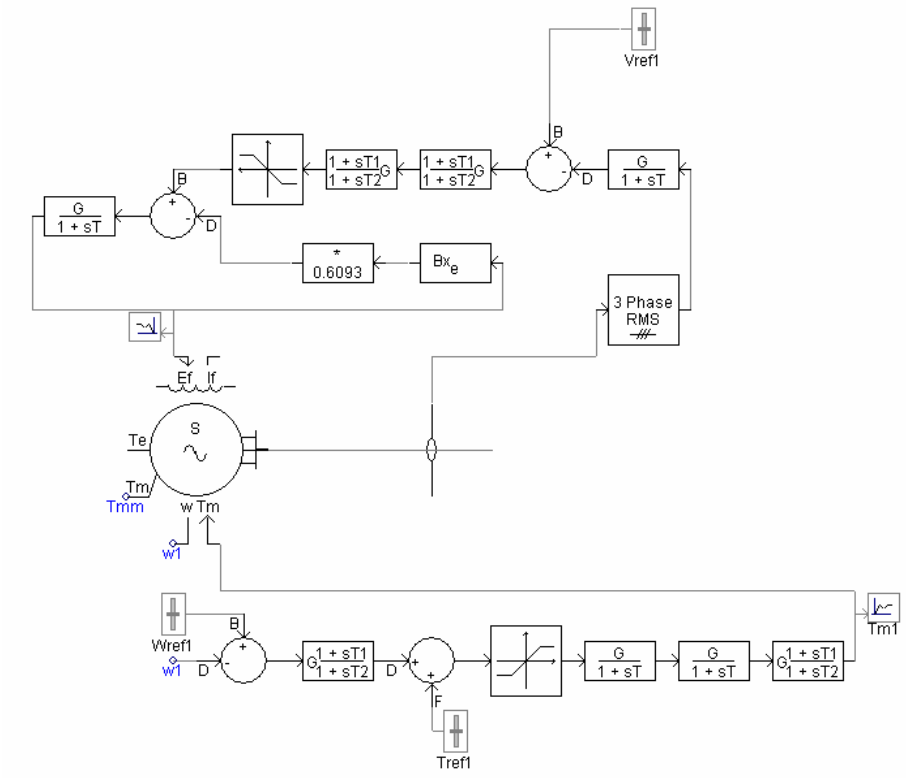

Figure 7-1: *Complete Generator Model in PSCAD/EMTDC.*

Excitation system and power system stabilizer are built according to features summarized in section 6.4.

7.2. Twelve Pulse Converters

Each converter of the HVDC link of the two area system (Figure 6-2) has been modelled in PSCAD/EMTDC using mainly two basic components available in its library. Firstly, a six-pulse bridge [32]. This component is a compact representation of a DC converter, which includes a built in 6-pulse Graetz converter bridge (can be inverter or rectifier), an internal Phase Locked Oscillator (PLO), firing and valve blocking controls and firing angle (α)/extinction angle (γ) measurements. It also

includes built in RC snubber circuits for each thyristor. For each converter two of these bridges connected in series are used.

The other component is a three phases, two windings transformer. This device represents a typical transformer based on the classical modelling approach. Figure 7-2 depicts the complete configuration of the rectifier converter.

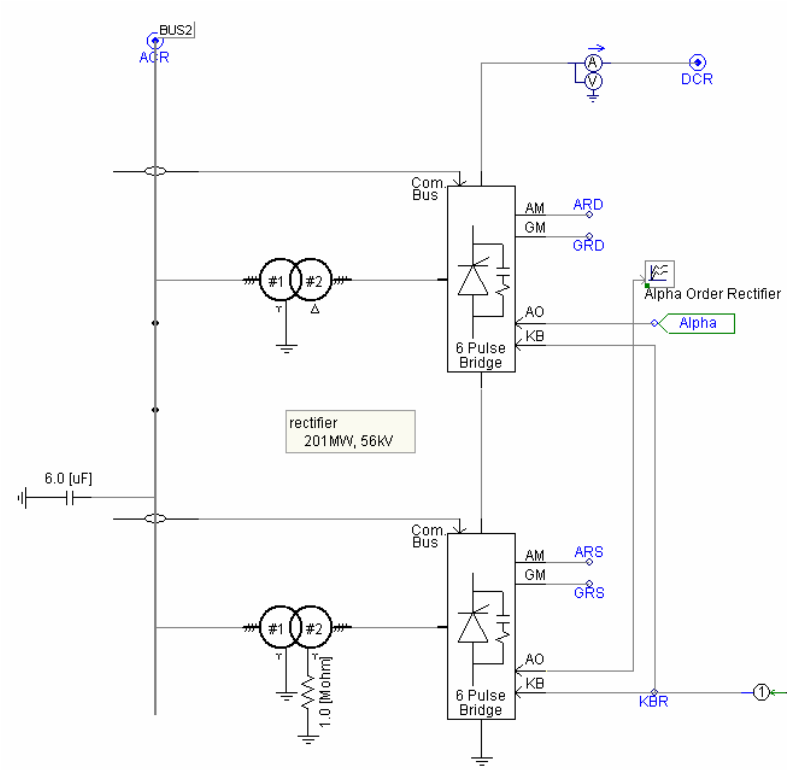

Figure 7-2: *Complete Converter Model in PSCAD/EMTDC.*

Suitable winding connections in each converter transformer are chosen based on reasons established in section 2.2. In the case of the six pulse bridges the option of RC snubber circuits for each thyristor is also chosen.

7.3. AC Transmission Lines

Transmission lines of the two area system have been represented in PSCAD/EMTDC using the Bergeron model [32]. The Bergeron model is based on a distributed LC parameter travelling wave line model, with lumped resistance. It represents the L and C elements of a PI Section in a distributed manner (i.e. it does not use lumped parameters). It is roughly equivalent to using an infinite number of PI Sections, except that the resistance is lumped (1/2 in the middle of the line, 1/4 at each end). Like PI Sections, the Bergeron Model accurately represents the fundamental

frequency only. It also represents impedances at other frequencies, except that the losses do not change. All parameters are set using the manual entry option available for the transmission line component. Figure 7-3 shows the configuration of the AC inter-ties of the two are system modelled in PSCAD/EMTDC.

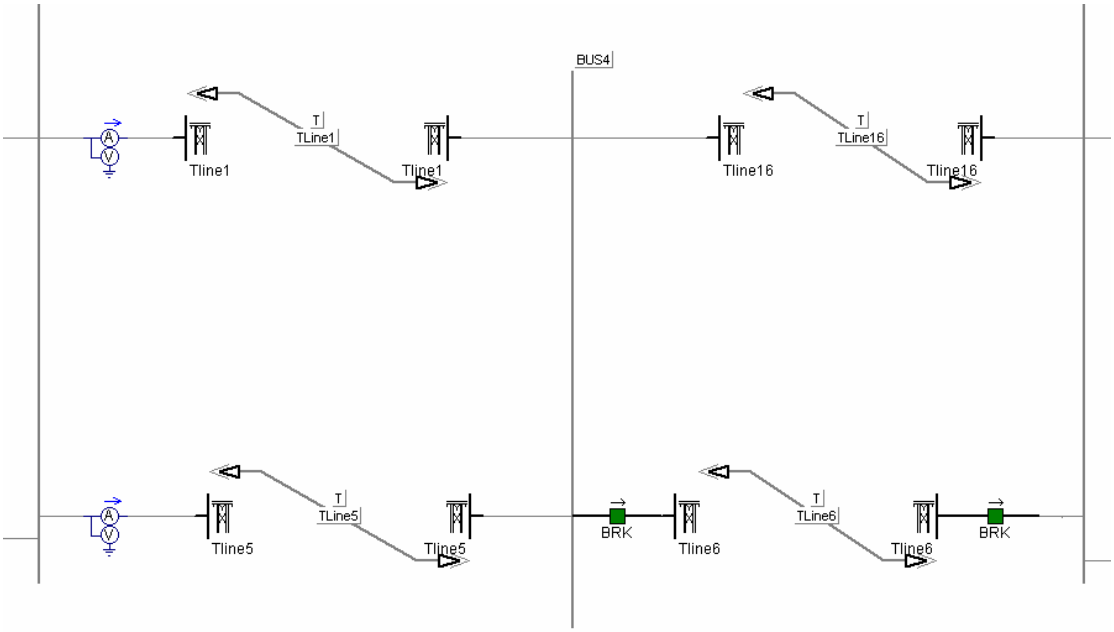

Figure 7-3: *AC inter-Ties Modelled in PSCAD/EMTDC.*

7.4. DC Inter-Tie

The HVDC link interconnecting the two areas of the study system is modelled in PSCAD/EMTDC using lumped parameters. Resistance and inductance components are the basic blocks of the DC line.

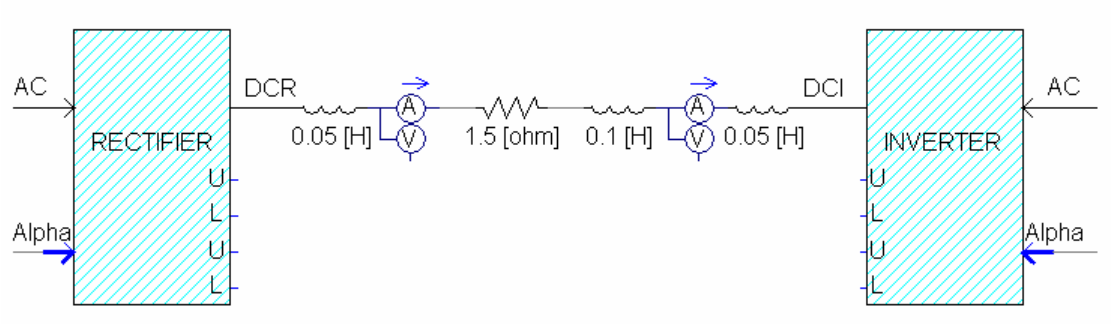

Figure 7-4: *DC inter-Tie Modelled in PSCAD/EMTDC.*

Figure 7-4 represents the HVDC link as is modelled in PSCAD/EMTDC along with the converters at each side of the two area system.

7.5. Loads

It has been stated before that the two are system includes two big load centres at each area (see section 6.2). These loads are represented in PSCAD/EMTDC using the fixed load component. This component models the load characteristics as a function of voltage magnitude and frequency, where the active and reactive powers are considered separately using the well known expressions [32]:

$$P = P_0\left(\frac{V}{V_0}\right)^a\left(1 + K_{pf}\Delta f\right)$$
$$Q = Q_0\left(\frac{V}{V_0}\right)^b\left(1 + K_{qf}\Delta f\right) \qquad (7\text{-}1)$$

Being P the equivalent load real power, P_0 the rated active power per phase, V the load voltage, V_0 the rated load voltage, a the voltage index for active power, K_{pf} the frequency index for active power, Q the equivalent load reactive power, Q_0 the rated reactive power (+inductive) per phase, b the voltage index for reactive power, and K_{qf} the frequency index for reactive power. Voltage index for active power ranges between 0.5 and 2 while voltage index for reactive power ranges between 1.5 and 5 [34], [35]. In the base case used in this work these two last parameters are set at 2 while the frequency indexes are set at zero. Cases considering variation of the voltage indexes are simulated and compared in section 9.5.

7.6. HVDC Link Controls

According to features described in section 6.3.1 the control structure of the HVDC inter-tie is modelled in PSCAD/EMTDC. Modelling is based upon the fundamental blocks found in the control system modelling functions (CSMF) folder of the master library of this platform.

For each converter control four main blocks are used, namely: generic current control block, generic gamma control block, voltage dependent current limits block, and minimum gamma detector block. The complete configuration for the control of one converter (inverter in this case) is depicted in Figure 7-5.

Regulators include in each control block have been adjusted by trial and error using the multi-run characteristic available at PSCAD/EMTDC, while voltage dependent current order limits have been adjusted according to the static characteristic shown in Figure 6-4.

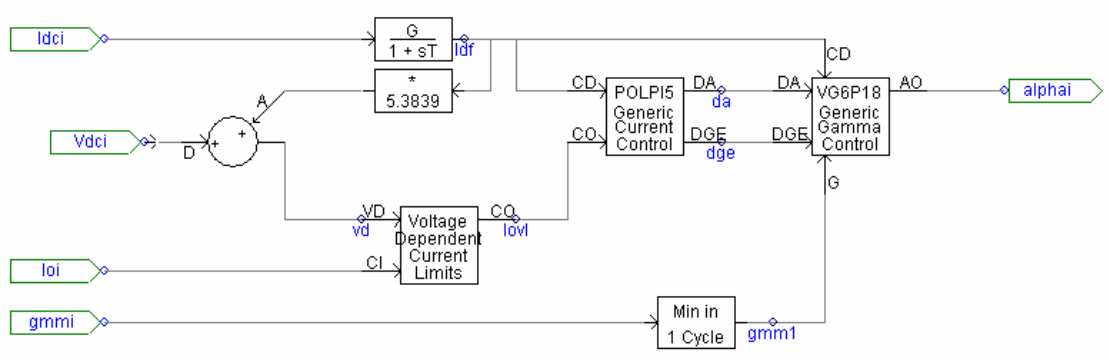

Figure 7-5: *Inverter Control Configuration in PSCAD/EMTDC.*

Once the control for each converter has been adjusted the master control, based on structured shown in Figure 6-5, has also been implemented in PSCAD/EMTDC.

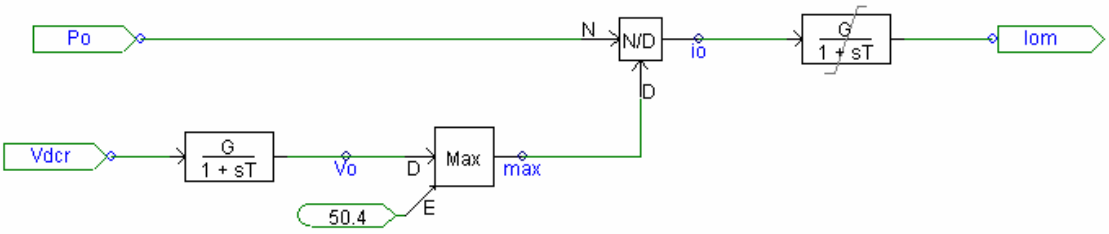

Figure 7-6: *Master Control Configuration in PSCAD/EMTDC.*

Figure 7-6 shows the complete configuration of the master control. The minimum voltage is fixed at 50.4 kV preventing in this way undesirable over-currents.

The whole basic control system of the HVDC inter tie in PSCAD/EMTDC is illustrated in the Figure 7-7. Scheme has been developed considering the features described in the section 6.3.1.

A slider block is used to setup the desired active power in the HVDC link. Once the active power has been fixed, the master power control determines the current orders needed and they are sent as inputs to the control of each converter. Using the current order sent by the master control and measured DC voltages and currents,

each converter control finds out the firing angle required as in the rectifier as in the inverter.

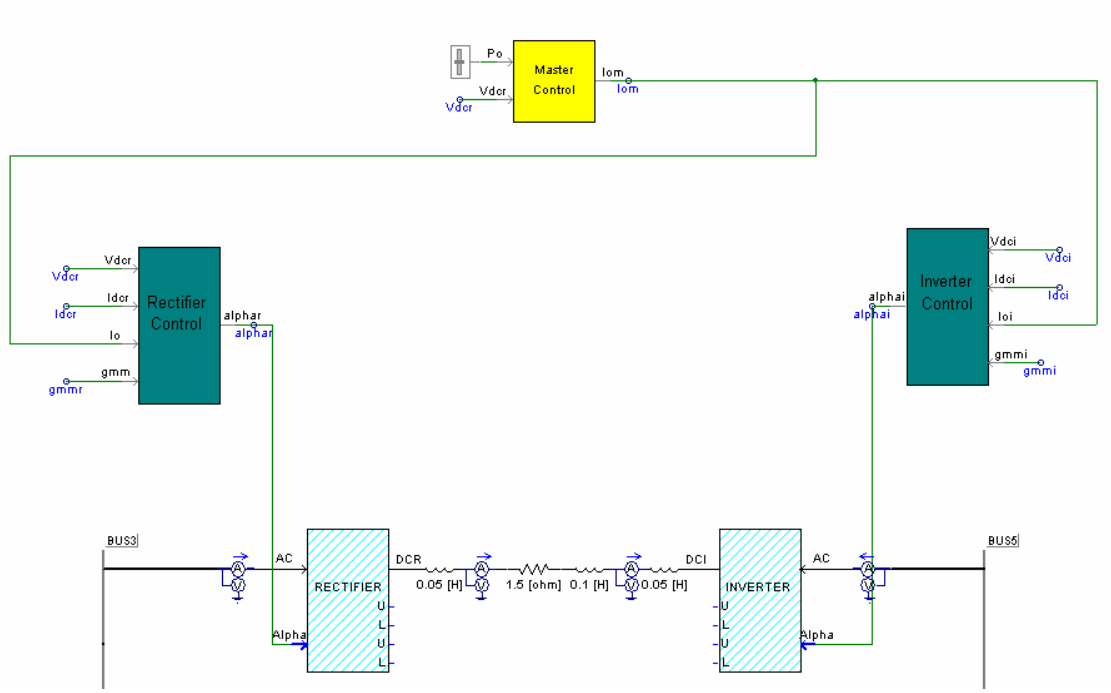

Figure 7-7: *HVDC Inter-Tie Control Configuration in PSCAD/EMTDC.*

8. Supplementary control

Power flow on DC transmission lines can be modulated by controlling the states of the converters at each end of the link. During a fault on a interconnected system, flows of oscillating power appears due to generators swings to new angles in response to accelerating or decelerating power [33]. If oscillating power flows are not attenuated, system instability emerges. The converter stations can be used to prevent this instability avoiding AC system separation and introducing damping improvement. Rapid discrete power changes (power modulation) can be used to improve transient stability while continuous proportional control is used to increase damping.

Transmission and generation systems configuration determine the relative effectiveness of the rapid DC power modulation. In particular, effectiveness is outstanding when the HVDC link is a major connection between two AC systems. This is the case of the two area system used in this work (see Figure 6-2).

Numerous studies related to power modulation of HVDC links have been reported showing effectiveness of the method. For instance, the pacific HVDC inter-tie (USA) includes a supplementary control system designed to modulate the power of the HVDC link [28]. This modulation damps the inter-area oscillations flowing in the parallel AC inter-tie; likewise, power modulation in the CU (North Dakota-Minneapolis-USA) HVDC system permits damping improvements [14].

8.1. Power Modulation of the HVDC Inter-Tie of Study System

In the case of the two area system shown in the Figure 6-2, three oscillation modes have been identified [26], [27]. Two of them correspond to local modes and the remaining one corresponds to an inter-area oscillation mode. One of the main goals in this work is to reduce the inter-area oscillation mode using the HVDC inter-tie features. Next table summarizes the values of the inter-are oscillation mode in AC transmission lines of the two areas power system, under different operation conditions. Modes are obtained through small signal analysis (see section 5) using MatNetEig[2] [26].

[2] MatNetEig is a MATLAB© based, object oriented program for small signal stability analysis of inter-connected power systems developed by Professor Graham J. Rogers.

Table 2 Inter-Area Oscillation Modes of Two Area System

	Case	Active Power Flow (MW)		Inter-area Mode		
		DC Tie	AC Ties	Eigenvalues	Frequency (Hz)	Damping Ratio
Without PSS	1	62	378	-0.017±j3.52	0.561	0.005
	2	100	338	-0.020±j3.57	0.569	0.0058
	3	200	240	-0.028±j3.62	0.576	0.0079
With PSS	1	62	378	-0.228±j2.50	0.398	0.091
	2	100	338	-0.237±j2.56	0.409	0.092
	3	200	240	-0.254±j2.58	0.411	0.098

Results presented in the foregoing table show damping improvement in the three cases studied once the power system stabilizer is added (time domain results will be expose in the next chapter). Albeit the damping ratio obtained adding power system stabilizers is acceptable ($\zeta \approx 0.1$), a safety margin is highly desirable [26]. This safety margin is attained using the HVDC link control system. The aim is to increase the damping ratio to a value close to 0.2.

As first step to achieve the aim described before, an observability study is performed. Using equations (5-9) and (5-10), and particularly the entries of the C' matrix (see section 5.1), observability levels of the different states of the two area system are established. Results from MagNetEig reveal that active power flow through the AC inter-ties is the most suitable signal for control purposes. The difference of frequency between the two areas of the system is also a possible feedback signal [26], but this case implies measurements at both sides of the HVDC link and a communication channel.

Thus, the most efficient feedback signal to the HVDC control system must be the total active power flowing in the parallel AC transmission lines. Consequently a supplementary control scheme for damping of inter-area oscillations must be based upon power modulation. Figure 8-1 illustrates the configuration of the closed loop control of the HVDC inter-tie using power modulation. The active power is measured in the AC inter-ties and then is used as input signal for the supplementary control block. Supplementary control block modulates the power signal and adds its result to the power order established for the HVDC link. The output signal of the supplementary control block is used to feed the master control block described before (see Figure 7-6). Finally master control generates the current order signals

required by the converter control blocks, which will command the rectifier and inverter at each end of the HVDC inter-tie.

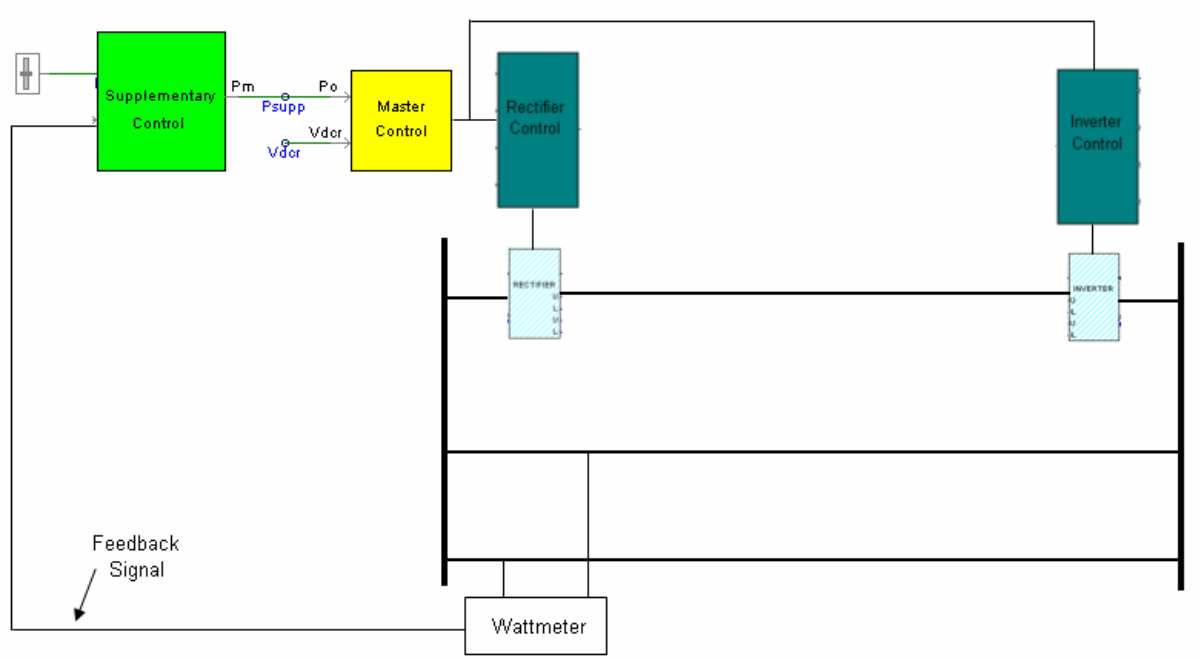

Figure 8-1: *Power Modulation Configuration.*

The design of the supplementary control block required in the configuration showed in the Figure 8-1 above, is developed according to the procedure described in the section 5.2. Considering results showed in the Table 2, the desirable eigenvalues location is that in which its frequency is around 0.4 Hz and the damping ratio around 0.2. Accordingly, the new location in the complex plane of the associated eigenvalues must be approximately λ_n=-0.513±j2.51 (see equation (5-13)). Hence the required shift in the direction of constant damped frequency is:

$$\Delta\lambda_i = -0.293 \qquad (8\text{-}1)$$

Thus, using equation (5-17) is possible to estimate the magnitude of the compensation loop once the residues of the eigenvalues have been determined. Residues are calculated using the expression (5-12) considering the power order given to the master control as the input and the active power flow through the AC lines as the output for each case listed in the Table 2. The representative value obtained following the described procedure is:

$$\begin{aligned} |R_i| &= 1.172 \\ \arg\{R_i\} &= 1.745 \end{aligned} \tag{8-2}$$

Therefore the compensator *H(s)* can be determined according to the general form (5-18) using the equations (5-17) and (5-19). Assuming that the number of lead-lag pairs is four and using the results (8-1) and (8-2), it is found that:

$$\begin{aligned} K &= |H(s)| = \frac{|\Delta\lambda_i|}{|R_i|} = 0.25 \\ \varphi_i &= \frac{\pi - 1.745}{4} = 0.349 \\ a_i &= \frac{1+\sin(0.349)}{1-\sin(0.349)} = 2.04 \\ \tau_i &= \frac{1}{2.51\sqrt{2.04}} = 0.279 \end{aligned} \tag{8-3}$$

Consequently the compensation block, according to (5-18), has the following form:

$$H(s) = 0.25\left[\frac{1+0.569s}{1+0.279s}\right]^4 \tag{8-4}$$

Finally, it is necessary to add a washout block to the compensator (8-4) in order to filter DC components. Washout time constant is set at 10 seconds. Then, the complete transfer function of the supplementary control block has the following form:

$$H(s) = 0.25\frac{s}{s+0.1}\left[\frac{1+0.569s}{1+0.279s}\right]^4 \tag{8-5}$$

Supplementary control block (8-5) has been modelled in PSCAD/EMTDC using CSMF library components.

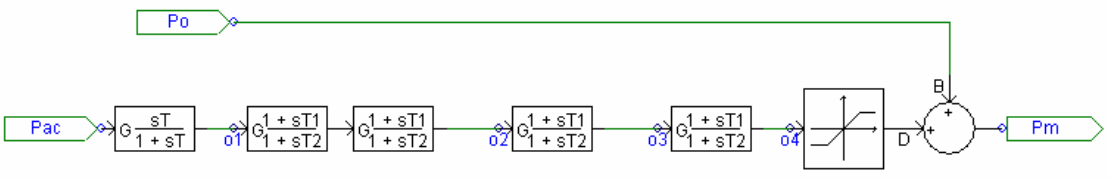

Figure 8-2: *Supplementary Control Configuration Implemented in PSCAD/EMTDC.*

The whole structure of the HVDC inter-tie along with its control modelled in PSCAD/EMTDC is illustrated in the next figure.

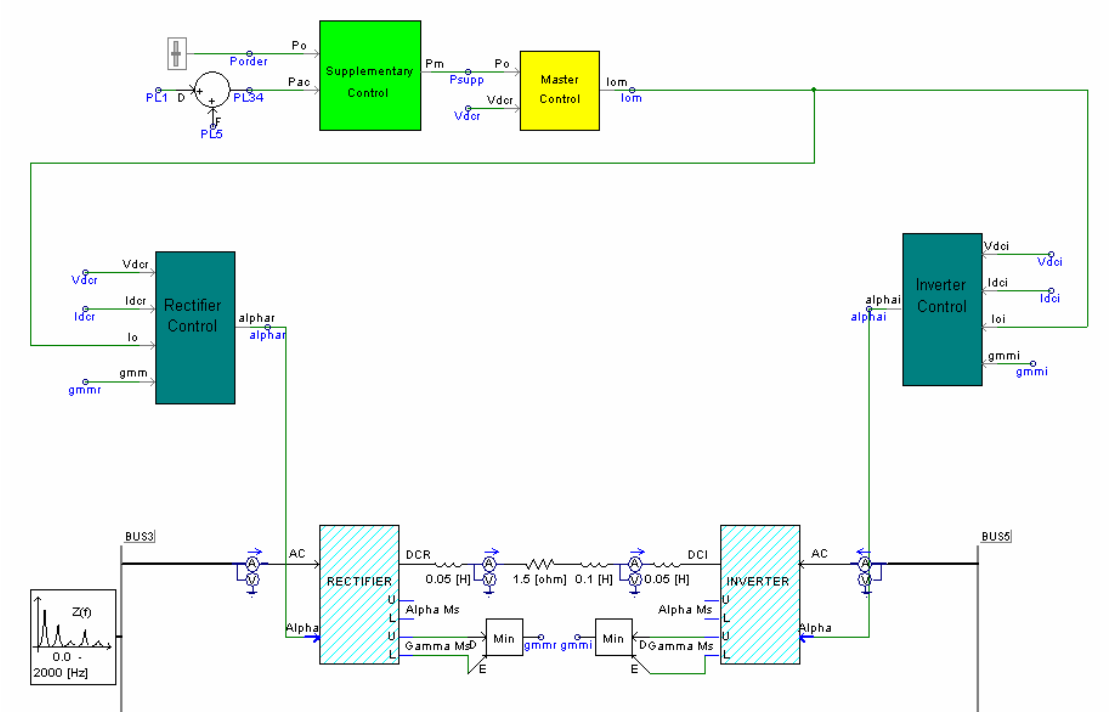

Figure 8-3: *HVDC inter-Tie and Its Control Implemented in PSCAD/EMTDC.*

9. Simulation results and analysis

Based upon structure described in foregoing chapters, the two area power system (Figure 6-2) has been modelled in PSCAD/EMTDC including the whole control scheme associated to the HVDC inter-tie. Next sections show the simulation results of the power system under different operative conditions and disturbances. Simulations have been focused on determining effectiveness of the supplementary control block in damping of inter-area oscillations.

9.1. Normal Operation

Parameters of the two-area system are set according to Table 1. Power order applied to the HVDC link is fixed at 200 MW. Initialization of the four generators is achieved identically maintaining them firstly as constant sources and then changing to generator representation at 0.5 seconds. After 0.8 seconds the machines are released and the system runs freely. Simulation is run during 120 seconds.

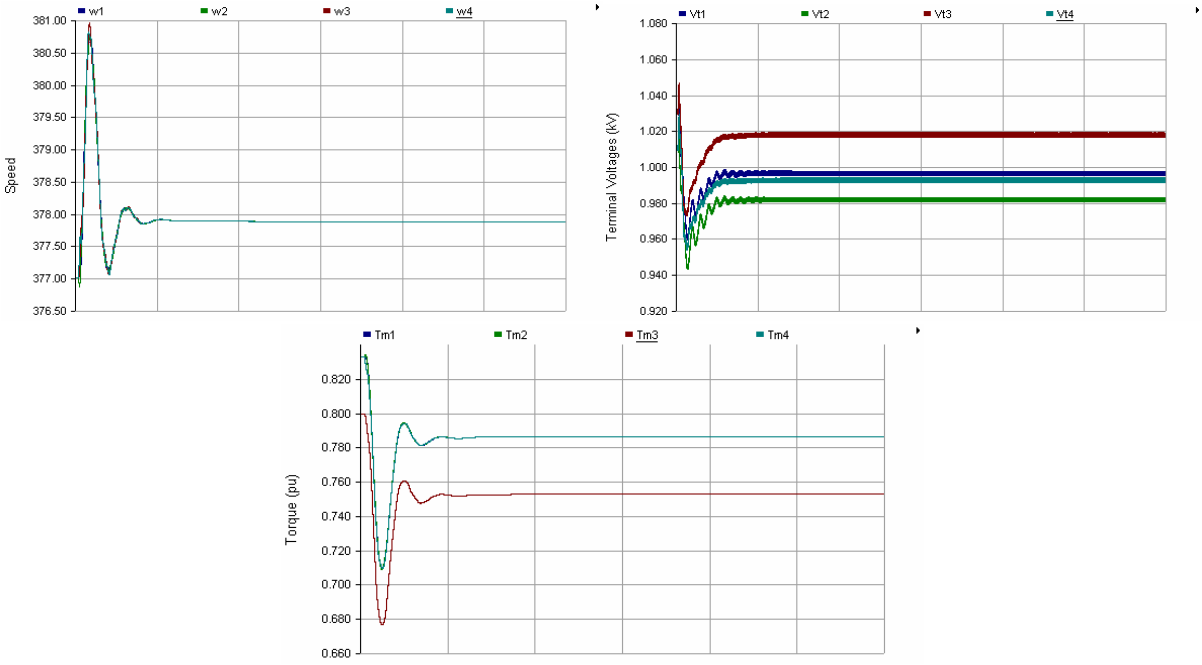

Figure 9-1: *Speeds, Terminal Voltages and Torques of the Four Generators of The Two-Area System.*

Figure 9-1 depicts the speed, terminal voltages, and torque responses of the four generators of the system. Oscillations are observed during the first few seconds

of the simulation, due mainly to the initialization process performed in each generator. Steady state is reached after 20 seconds approximately.

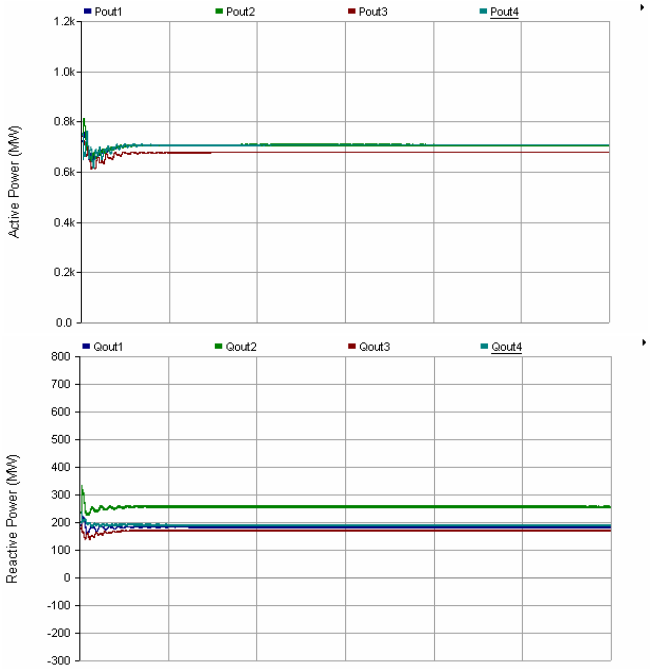

Figure 9-2: *Active and Reactive Power from the Four Generators of The Two-Area System.*

Figure 9-2 shows the active and reactive power generated by each machine of the system. Units 1, 2, and 4 supply 704 MW each one, while unit 3 supplies 674 MW. Thus, total active power generated is around 2786 MW. According to Table 1 the real power of the load sums 2734 MW. Hence, total losses of the system under these conditions are around 52 MW. On the other hand, reactive power supplies are 180 MVAr, 254 MVAr, 166 MVAr, and 186 MVAr respectively. Being consequently supplied in total to the power system 786 MVAr.

In both, active and reactive power cases, production is bigger in area 1 (see Figure 6-2) than the other side. Thus, power is exported from area 1 to area 2. Figure 9-3 illustrates how the exported active power is distributed through the three transmission lines interconnecting both areas. In the case of the HVDC link its power has been fixed before being quite close to 200 MW. In the case of the AC inter-ties, the rest of the exported power is distributed equally being approximately 113 MW.

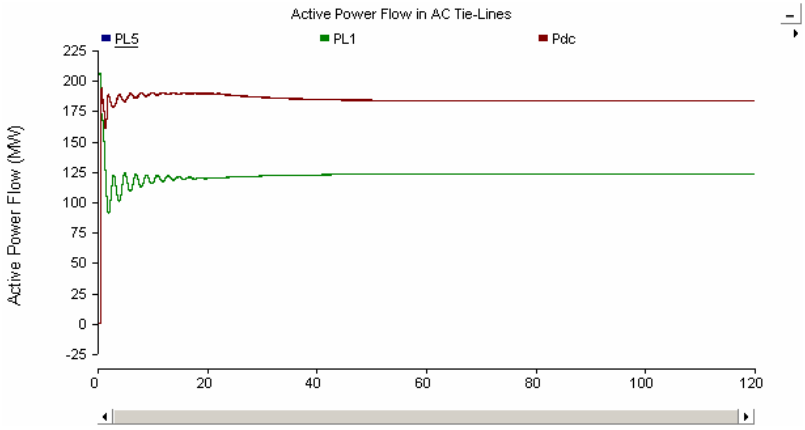

Figure 9-3: *Active Power Flow Through DC and AC inter-Ties.*

Figure 9-4 shows the currents and voltages of the HVDC link measured in both the rectifier and inverter sides.

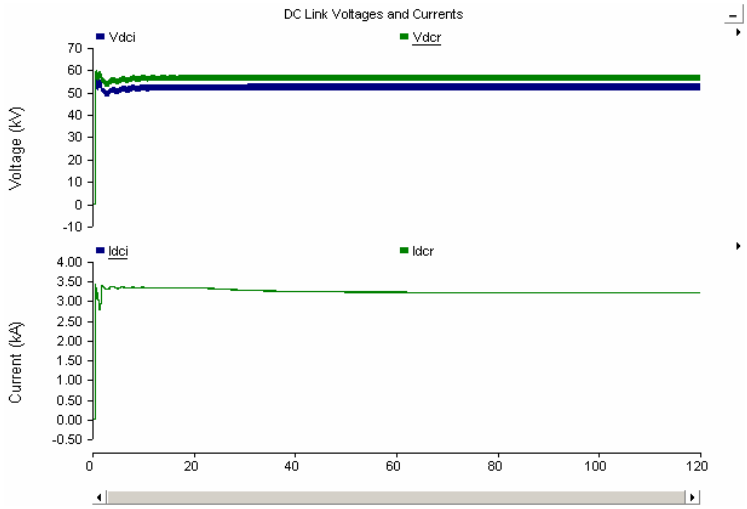

Figure 9-4: *DC Voltages and Currents at Both Sides of the HVDC Link.*

9.2. Three Phase Fault at AC Inter-Tie

A three phase fault is simulated into the study power system. Fault is applied to one of the AC inter-ties as is illustrated in the Figure 9-5. Fault is considered permanent and is cleared isolating the AC inter-tie section affected. The action of protection system takes around 80 ms. Two cases are considered, one including the supplementary control block and other without it.

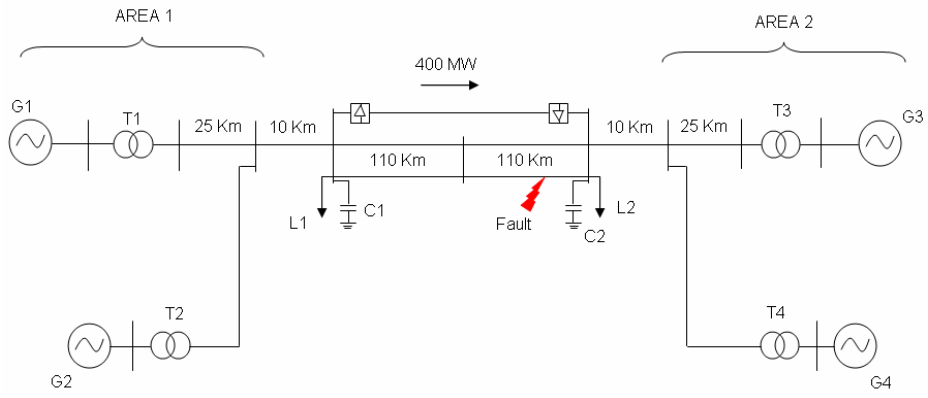

Figure 9-5: *Fault in the Two-Area System.*

Considering the fact that the power circulating through the AC inter-ties will be the magnitude modulated by the compensation loop of the HVDC control (see Figure 8-1), it is desirable to study its behaviour after a fault. Figure 9-6 sketches this behaviour when the HVDC system includes only basic control structure (Figure 7-7).

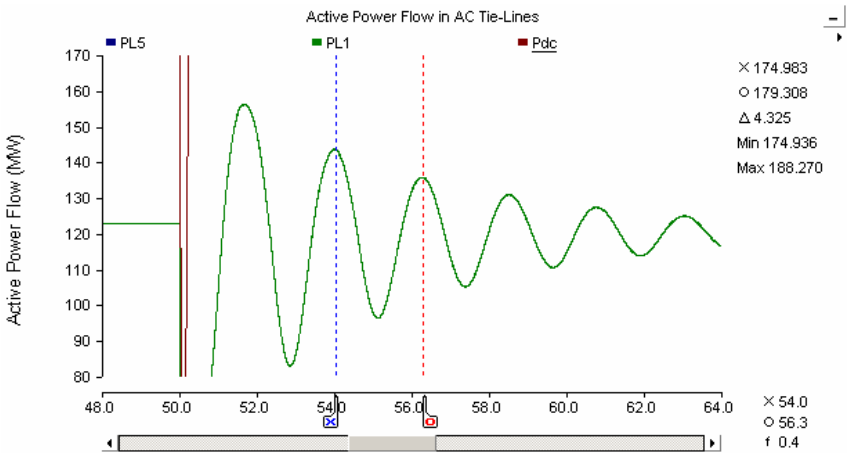

Figure 9-6: *Active Power Flow Through AC Inter-Ties After a Three Phase Fault.*

Active power flow through the AC lines clearly shows an oscillatory response, being the frequency of this oscillation around 0.4 Hz. This low frequency value confirms that the oscillations correspond to inter-area electromechanical oscillations in which group of generators of area 1 swing against group of area 2.

Furthermore, the frequency of the inter-area oscillations agrees with that obtained from small signal analysis and chosen to design the supplementary control block (see section 8.1). Figure 9-7 contrasts the response of the system considering the compensation loop modulating active power through the HVDC link and the response without the supplementary control.

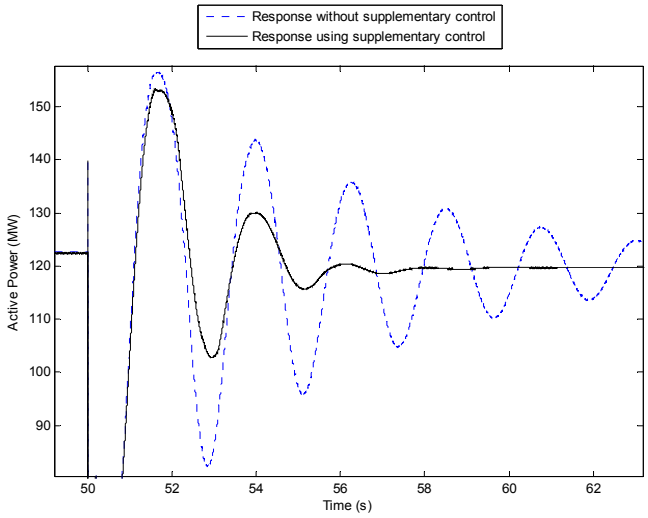

Figure 9-7: *Active Power Flow Through AC Inter-Ties After a Three Phase Fault.*

Effectiveness of the designed compensator is clearly showed in the graph above. An important rise of the damping is achieved improving in this form the stability of the system overall. Inter-area oscillations are reduced swiftly although the system is operating under stressful conditions.

System operating with only power system stabilizers and basic control at the HVDC link presents insecure damping levels. After the three phase fault, even though the oscillations are damped, they remain in the system for relatively long periods (over 40 seconds). In contrast, when the supplementary control loop is added to the basic control structure of the HVDC inter-tie, a secure high damping level is reached, reducing not only the amplitude of the electromechanical inter-area oscillations but also their duration. Figure 9-7 shows how the steady state condition is recovered in this case in approximately 8 seconds.

Figure 9-8 shows the changes of the generators' speed after the fault. Graphs show clearly the action of the supplementary control of the HVDC link. Oscillations are damped in all the machines, being notorious the effect over the generators in area 2, where oscillations are pronounced.

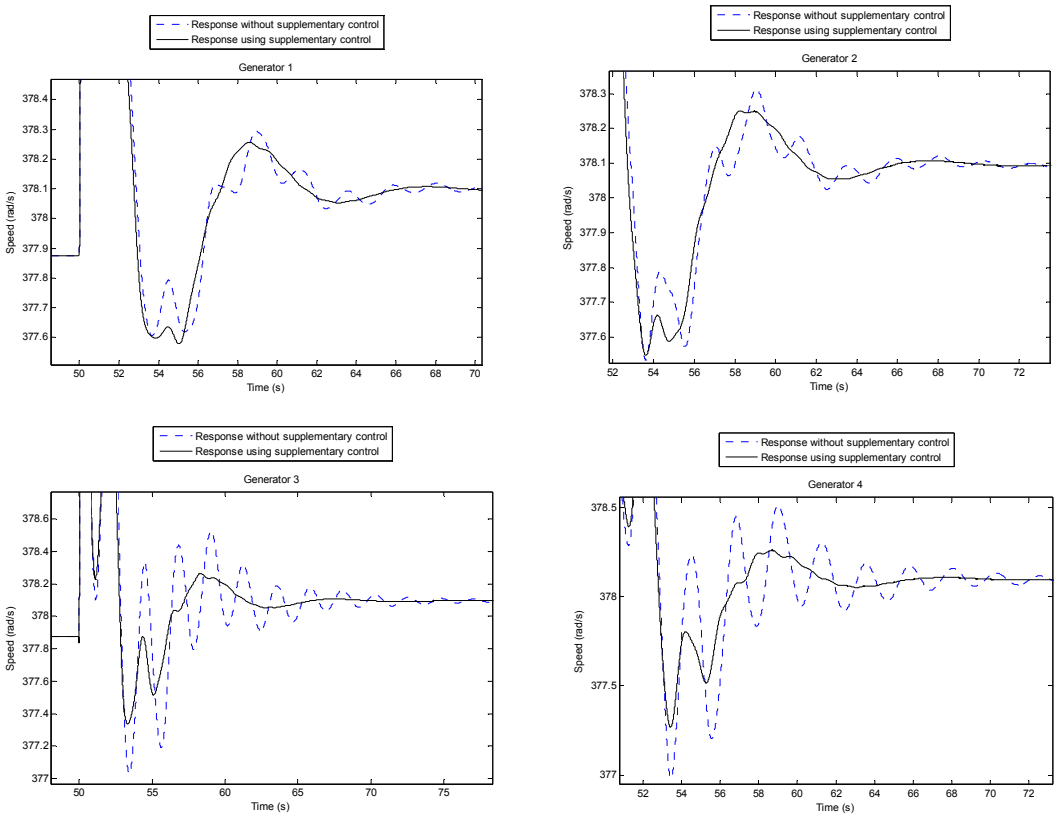

Figure 9-8: *Generators' Speeds After a Three Phase Fault.*

Figure 9-9 depicts the voltages at the terminals of each generator. A strong increment in the damping is attained once the compensation block of the HVDC control system is activated. Power modulation permits terminal voltages of each machine to return rapidly to the pre-fault conditions. In contrast to the case of the speeds of the generators (Figure 9-8), where oscillations are higher at area 2, oscillations in terminal voltages are much more prominent at area 1 of the power system.

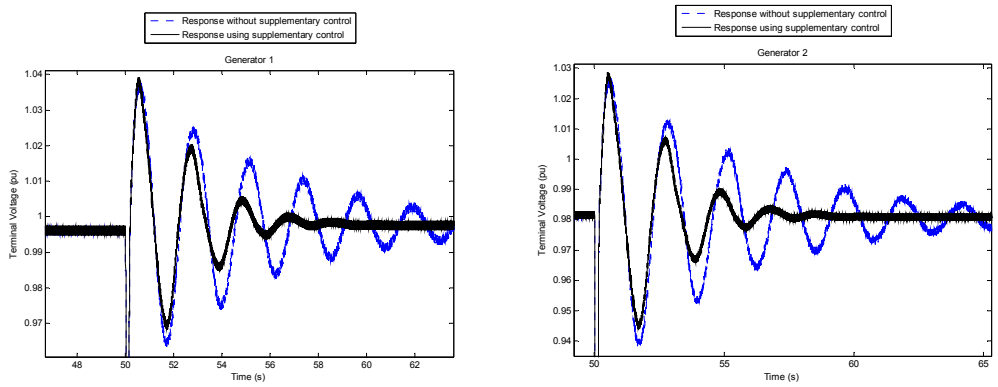

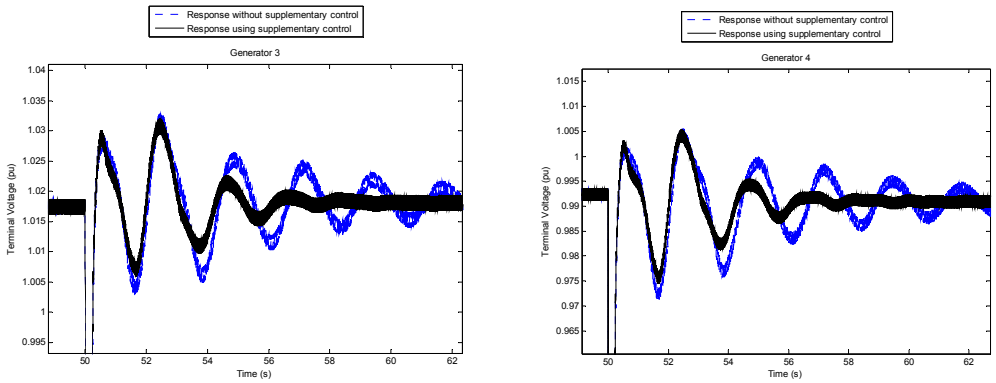

Figure 9-9: *Generators' Terminal Voltages After a Three Phase Fault.*

Considering the same fault condition illustrated in the Figure 9-5 others simulations are run, varying the total active power circulating through the HVDC inter-tie. Two cases are simulated: 90 MW and 60 MW.

Figure 9-10 and Figure 9-11 sketch the outcomes when the active power through the HVDC link is set at 90 MW. Those show the response of the power transfer through the AC lines along with the variation of the speeds at each machine of the system. Alternatively, Figure 9-12 and Figure 9-13 reveal the same responses but for the case of 60 MW. Each case considers the response including the supplementary control and also excluding it. Similitudes are evident between the responses obtained before for the case of 200 MW and those derived when the DC power is set at 90 MW. A clear increment in the damping is noted in both cases when the power modulation is performed using the supplementary control loop. Settling times in both cases are similar (around 8 seconds) showing the effectiveness of the compensation loop although the HVDC inter-tie is operating near to the half of its capacity.

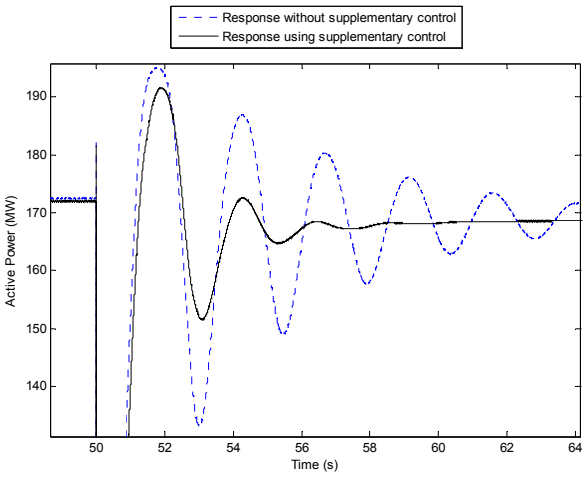

Figure 9-10: *Active Power Flow Through AC Inter-Ties After a Three Phase Fault (P_{dc}=90MW).*

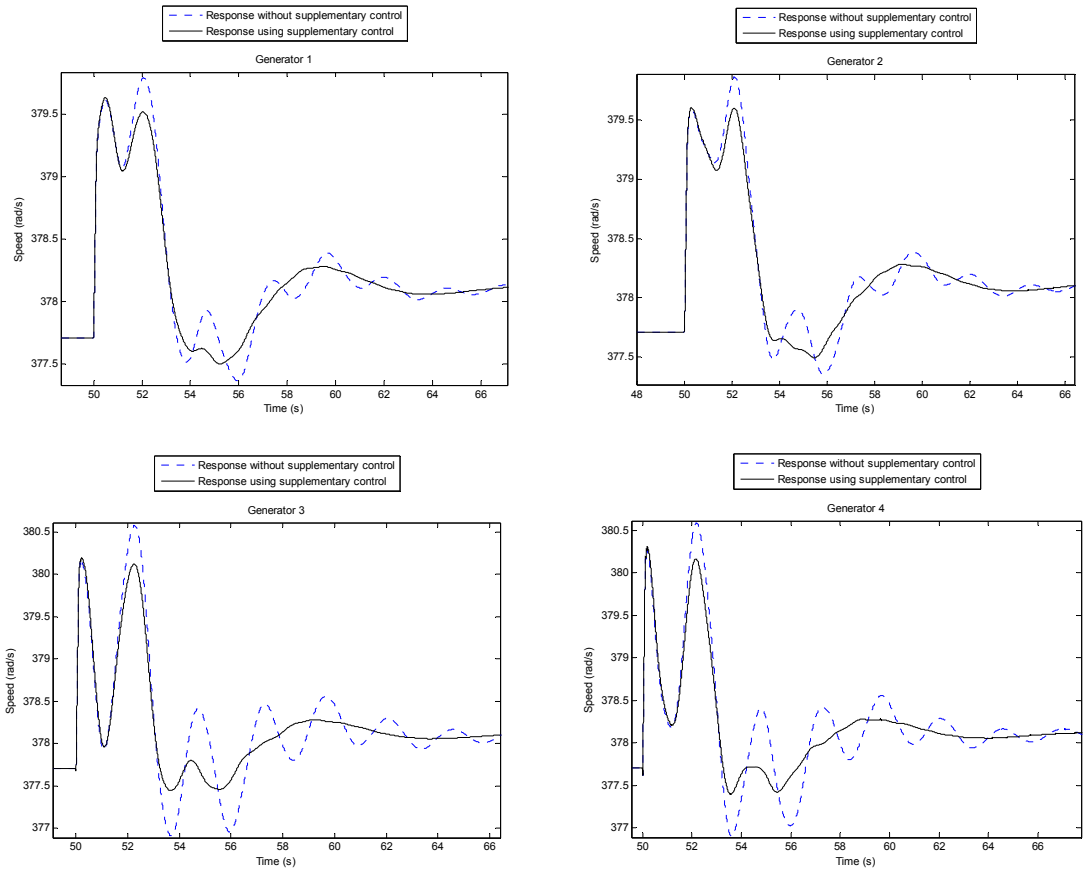

Figure 9-11: *Generators' Speeds After a Three Phase Fault (P_{dc}=90MW).*

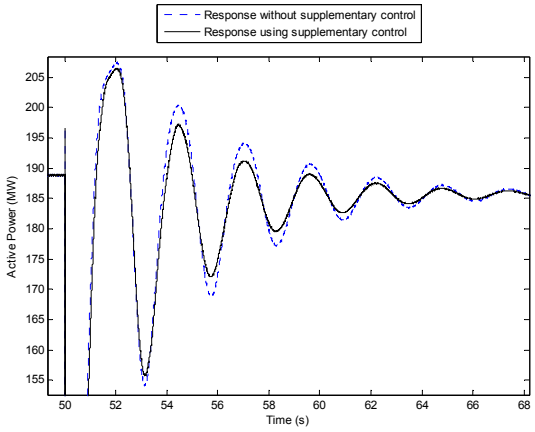

Figure 9-12: *Active Power Flow Through AC Inter-Ties After a Three Phase Fault (P_{dc}=60MW).*

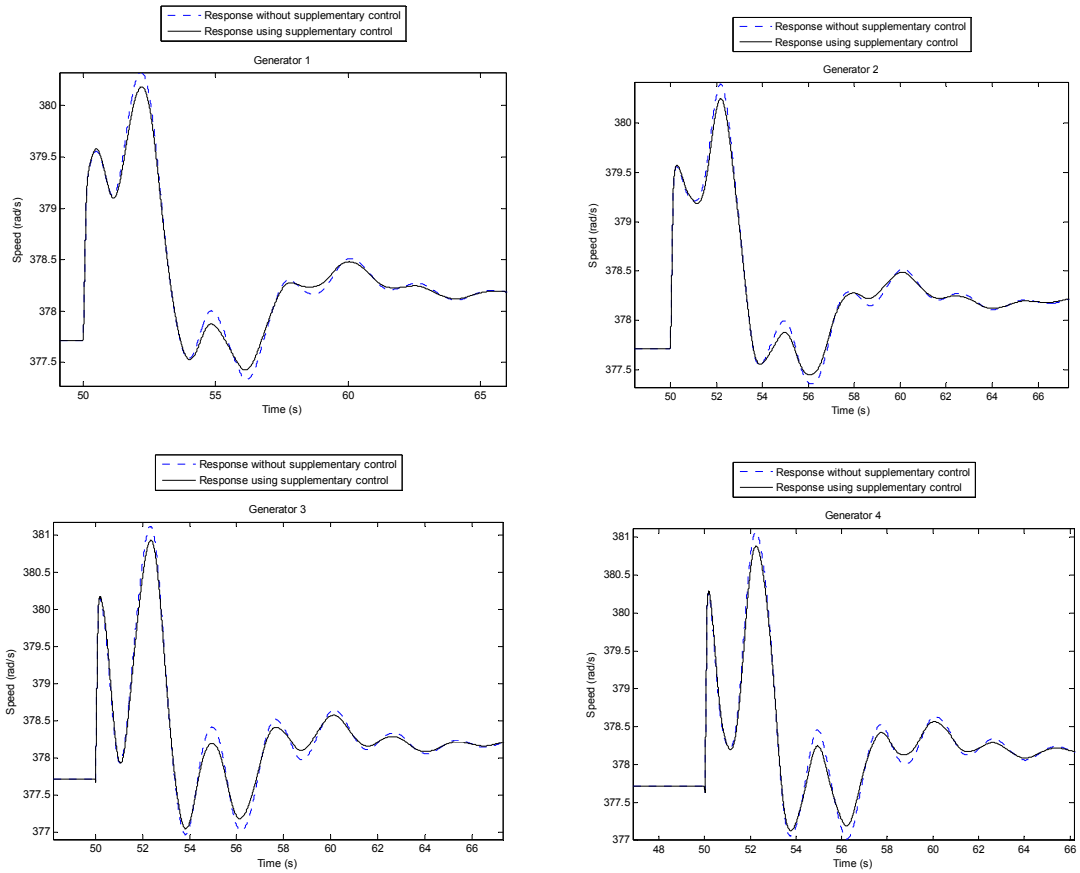

Figure 9-13: *Generators' Speeds After a Three Phase Fault (P_{dc}=60MW).*

In contrast, the responses of the power system obtained for the case of 60 MW (Figure 9-12 and Figure 9-13) show only a slight improvement of the damping of the inter-area electromechanical oscillations when the supplementary control is

activated. In this case the effect of the power modulation has lower impact in the system due to the small power circulating through the HVDC inter-tie. Hence, contribution of the control of the HVDC link to the improvement of the damping is very poor.

9.3. DC Fault at Inverter Side of the HVDC Inter-Tie

A fault is applied over the HVDC inter-tie near to the inverter (Figure 9-14). Duration of the fault is set at 0.1 seconds.

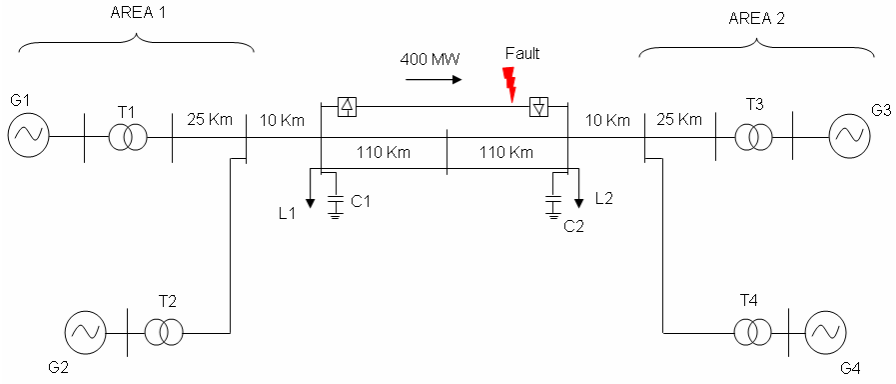

Figure 9-14: *DC Fault in the Two-Area System.*

Figure 9-15 represents the response of the active power transfer between the two areas of the power system after the fault event. A pronounced peak appears immediately after the DC fault when the power circulating the DC link is partly transferred to the AC transmission lines. This peak is followed by an oscillatory behaviour associated with the electromechanical inter-area modes. Continuous black curve, corresponding to the response with the supplementary control loop, shows the damping improvement of the system when is compared with the case in which only the basic control structure of the HVDC link is used (dashed blue curve). The increment of the damping ratio is similar to cases studied in section 9.2 and quite close to the value established in the design of the compensator (around 0.2).

Changes in the DC current levels of the HVDC transmission line after the disturbance are illustrated in the Figure 9-16. Particularly interesting are the variations introduced by the supplementary control loop in order to achieve power modulation (continuous black curve in the figure). Robustness of the HVDC link and its control structure permits to perform these stiff and swift changes. Figure 9-17 shows the impact of the power regulation over the speeds of the generators of the system.

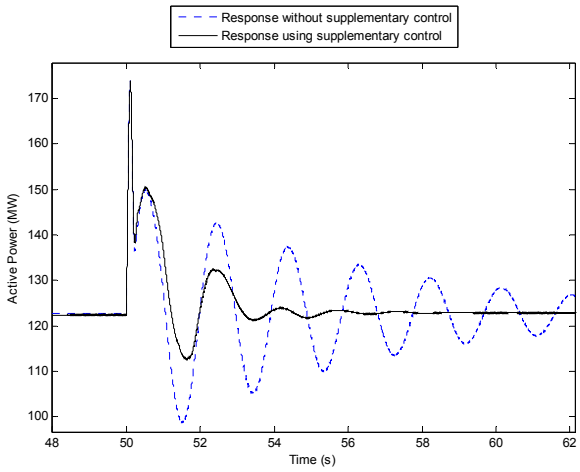

Figure 9-15: *Active Power Flow Through AC Inter-Ties After a DC Fault.*

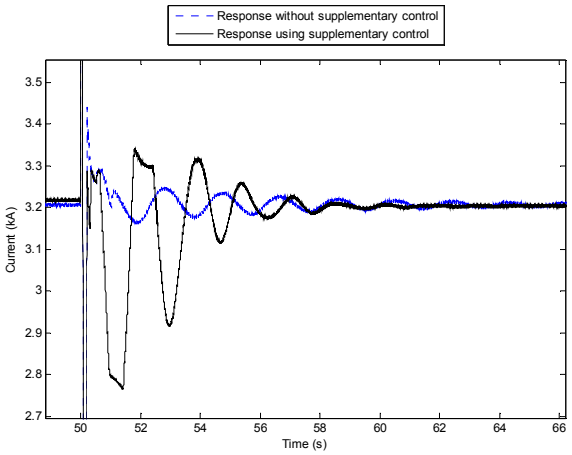

Figure 9-16: *DC Current After a DC Fault.*

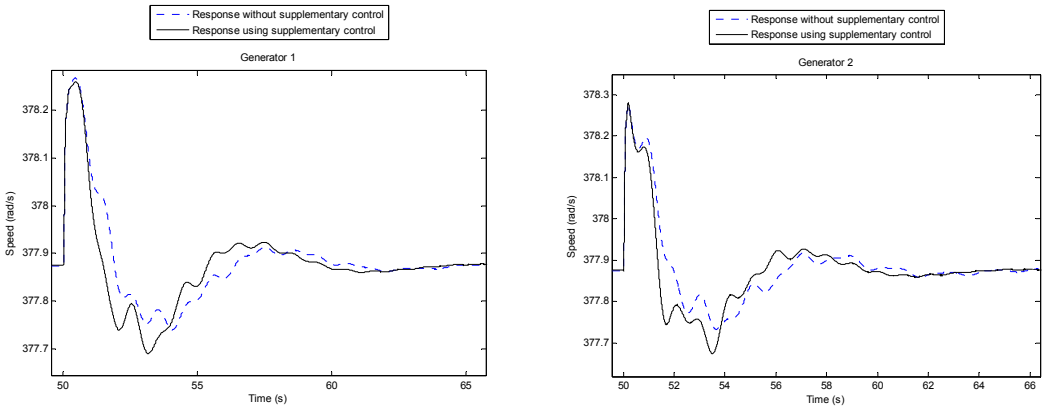

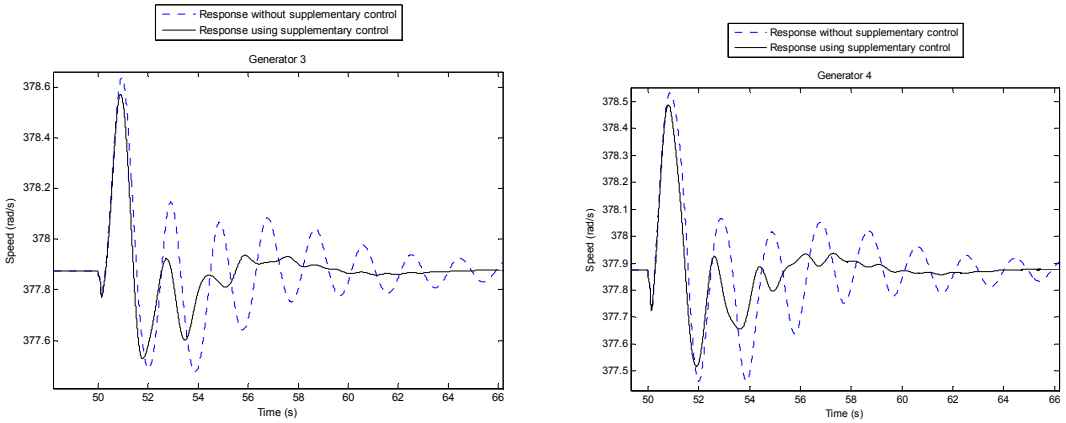

Figure 9-17: *Generators' Speeds After a DC Fault.*

9.4. Fault in 10 Km AC line in Area 1

A three phase fault with duration of 0.1 seconds is applied to the 10 Km AC line, which interconnect generators to inter-ties in area 1 of the study power system (Figure 9-18).

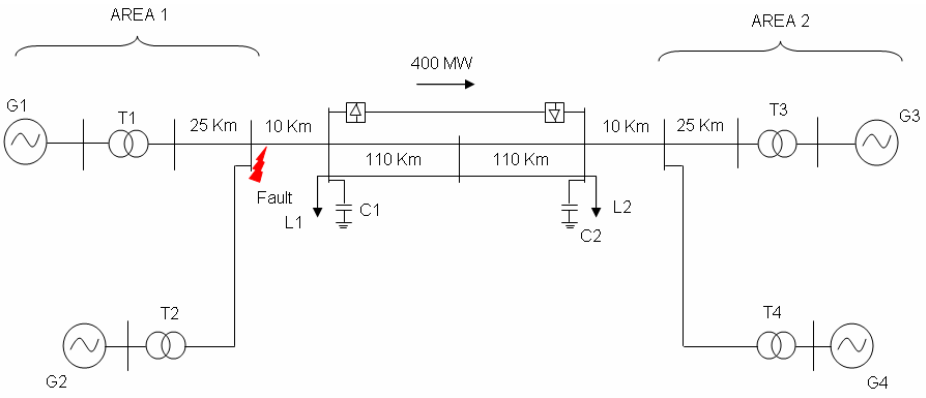

Figure 9-18: *Fault in the Two-Area System.*

Responses of the system after the fault event are presented in Figure 9-19, Figure 9-20, and Figure 9-21. Increase of damping of inter-area oscillations, when the compensation loop is added, is also observed in this case, even though the system is operating under stress conditions and the disturbance affects considerably the power supply. This reflects the robustness of the supplementary control system implemented over the basic control of the HVDC inter-tie.

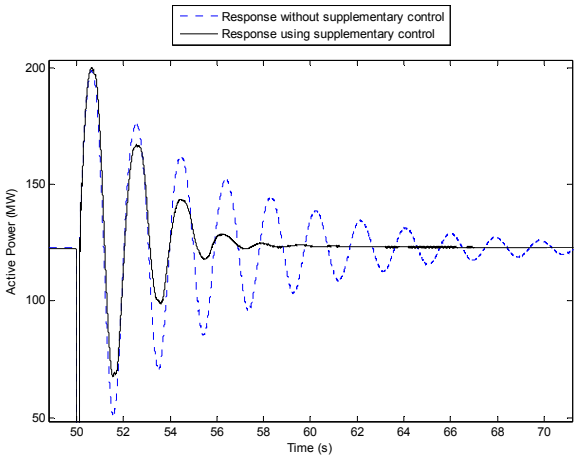

Figure 9-19: *Active Power Flow Through AC Inter-Ties After a Three Phase Fault.*

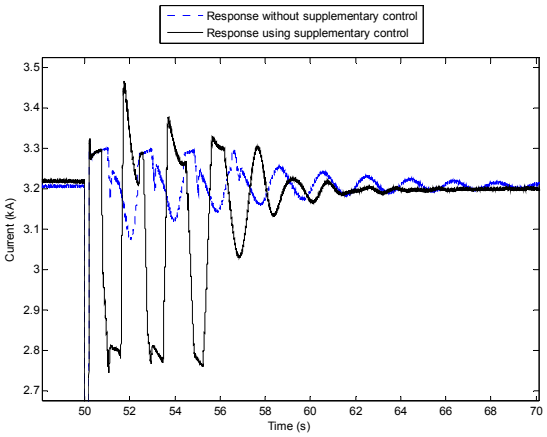

Figure 9-20: *DC Current After a Three Phase Fault.*

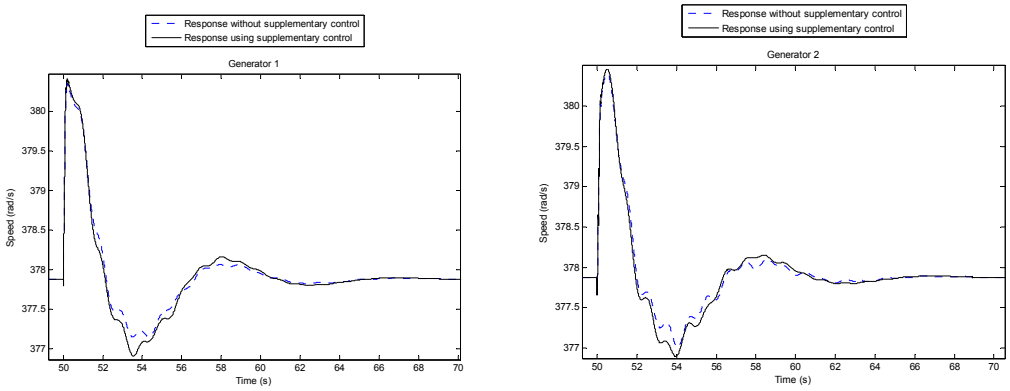

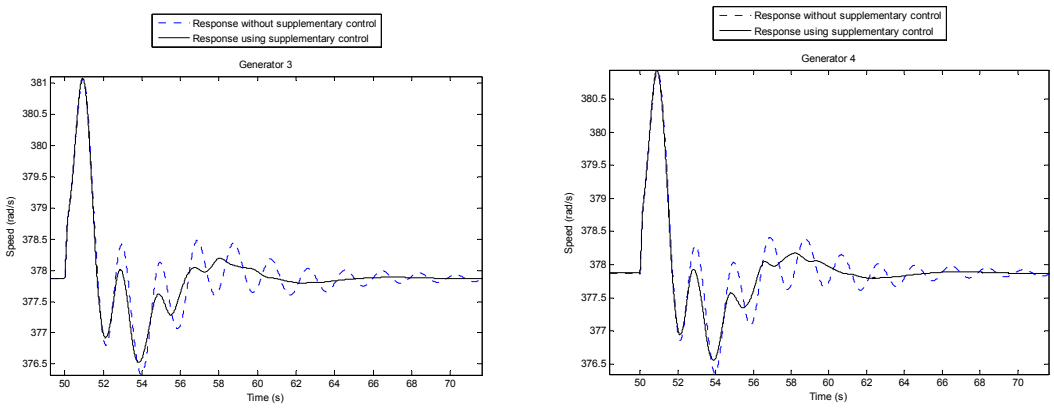

Figure 9-21: *Generators' Speeds After a Three Phase Fault.*

9.5. Responses Considering Different Load Characteristics

Importance of load characteristic modelling in the inter-area oscillation phenomenon has been widely reported [27], [34], and [35]. In order to determine the effect of the variation of the load characteristic over the supplementary control scheme performance, a series of simulations have been run changing the voltage indexes of the load (see section 7.5). These indexes are nearly equal to the variation of the active or reactive power with respect to the voltage variation (dP/dV or dQ/dV) [35].

Voltage indexes are varied at both load centres of the power system in each case. Once the indexes have been changed, the same fault condition used in the section 9.2 is simulated. In each case the supplementary control loop is maintained operating. Figure 9-22 illustrates the response of the system after the three phase fault for several static load characteristics.

A clear effect over the electromechanical inter-area oscillations is shown due to the load variations. Three cases are easily identified. Firstly, the case when the voltage index for the active power is low (α=0.5). In this case, the damping of the system is reduced dramatically and the supplementary control loop modulating the power over the HVDC link is ineffective. The second notorious case is represented by the results corresponding to the voltage index for the active power equals to one. In those cases there is also a decrement in the damping of the system but now the compensation loop of the HVDC link is able to increase it, modulating the power. Thus oscillations are damped keeping the system stable. However, the damping process is less effective that those observed in the third group of simulations. The third case regards a voltage index for the active power equals to two and different

values for the index of the reactive power. Responses grouped in this case are quite similar to the base case studied in the section 9.2 (a=2, b=2); namely, electromechanical inter-area oscillations are effectively damped by the power modulation through the HVDC inter-tie and thus the system recovers its pre-fault condition swiftly.

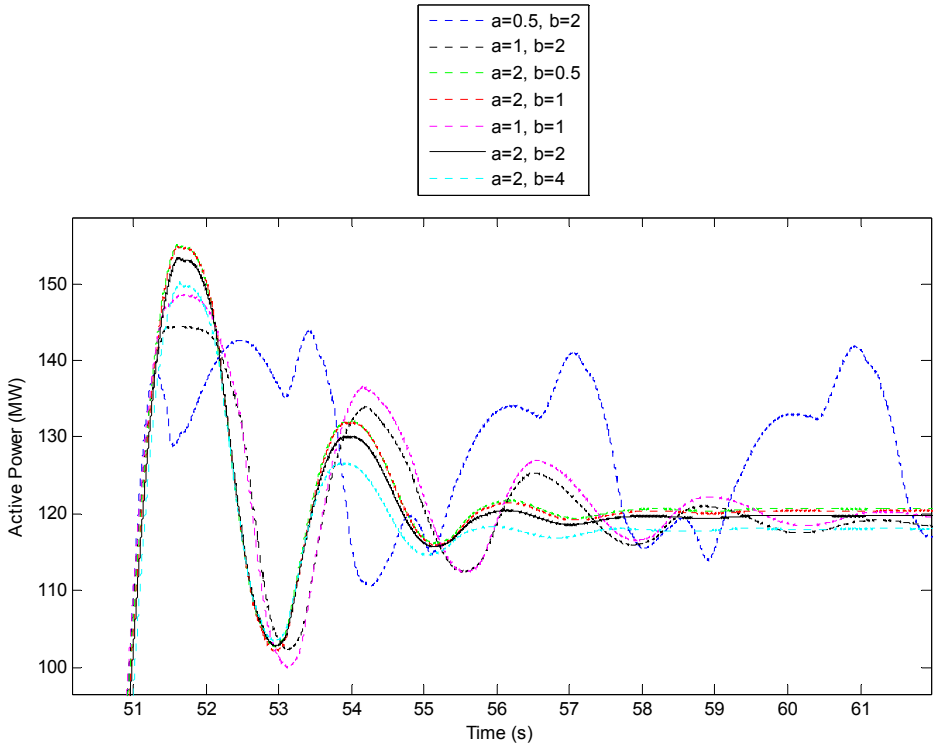

Figure 9-22: *Active Power Transfer After a Three Phase Fault Considering Different Load Characteristics.*

Consequently, the designed supplementary control loop for power modulation is more sensitive to variations of the voltage index for active power. If the composite load characteristic is predominantly reactive, namely: low variation of the active power with respect to the variation of the voltage (dP/dV) and high variation of the reactive power with respect to the variation of the voltage (dQ/dV), then the response of the power modulation of the HVDC link is limited and ineffective. Alternatively, the supplementary compensator added to the HVDC inter-tie is highly effective when the voltage index for active power is above one, notwithstanding the variations of the voltage index for reactive power.

Similar conclusions have been derived maintaining fixed the parameters of the load in the area one of the system while the indexes are changed in the area two.

Thus, variations of the static load characteristic in the area two (receiving end) have a notorious impact in the inter-area electromechanical oscillations behaviour, being the scope of action of the supplementary control loop of the HVDC link similar to that described before. Figure 9-23 shows the response of the active power transfer after the fault when voltage indexes of the load in the area 2 of the power system are changed.

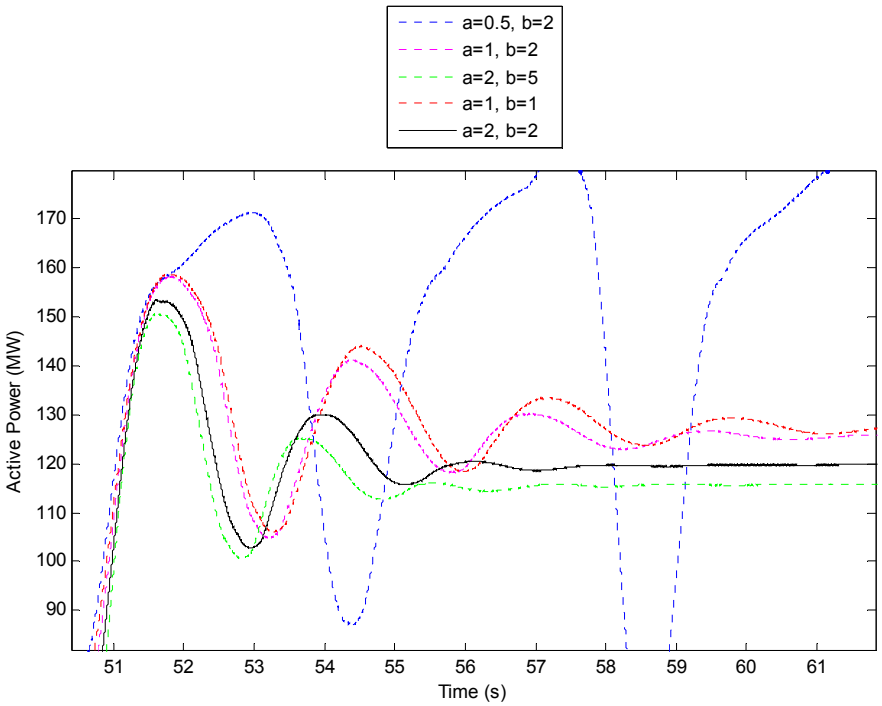

Figure 9-23: *Active Power Transfer After a Three Phase Fault Considering Different Load Characteristics only in Area 2 of the System.*

A similar impact of the variations of the static load characteristic in the electromechanical inter-area oscillations mode of the two area system with only AC inter-ties have been reported [27]. Nonlinearities in the load of the receiving end of the system (area two) reduce drastically the damping of the system while the effects are opposite when the variations are applied to the load in the sending end (area one).

10. Conclusions

Results obtained from two-area power system show how the control over the HVDC inter-tie effectively reduces the electromechanical inter-are oscillations. The supplementary outer control loop of the HVDC link, suitably designed, permits to increase the damping ratio of the system to a safe value, which can not be attained solely using power system stabilizers. Damping improvement is achieved modulating active power circulating through the HVDC link.

Scope of the supplementary control loop of the HVDC inter-tie has been evaluated revealing two important conclusions. Firstly, the effectiveness of the linear analysis; small signal analysis used to develop the compensation loop studying local behaviour around an operation point is further extensive to other operation conditions. Thus, although the supplementary control scheme has been designed under certain specific conditions, its functionality is quite far applicable to several other operative conditions of the system, not only in terms of disturbances but also in power transfer and even load characteristics.

Secondly, the sensitivity of the supplementary control loop of the HVDC inter-tie to the composite static load characteristic. Power modulation through the HVDC link effectively reduces electromechanical inter-are oscillations under a wide range of composite static load characteristics. Response is however limited by the value of the voltage index for active power; the compensation loop is functional only when this index is greater than one, no matter the value of the index for reactive power. Values of this index above one are typical in residential and commercial load types. Additionally, results show that the effectiveness of the supplementary control scheme is barely affected by the value of the voltage index for reactive power; this is an important result due to the fact that practical reactive power characteristics are more variable depending on several and sometimes unknown factors.

11. Future Work

The development of supplementary control schemes based upon frequency modulation can be stated as an interesting future work. This type of modulation is widely used in real HVDC links in order to reduce inter area oscillations. Using more complex models and in general the same procedure described here, extensive studies can be achieved evaluating the possibilities of the HVDC links in the AC power system.

Another interesting topic would be to attain a comparative study of the responses of the supplementary control systems of the HVDC links developed under other different techniques. For instance, H-infinity or frequency responses based techniques.

Bibliography

[1] J. Arrillaga. *High Voltage Direct Current Transmission.* Vol 6, London: Peter Pereginus Ltd., 1983.

[2] V.K. Sood. *HVDC and Facts Controllers*. USA: Kluwer Academic Publishers, 2004.

[3] N. Mohan, T. Undeland, W. Robbins. *Power Electronics*. USA: John Willey & Sons, 2003.

[4] F. Nozari, H. Patel. "Power Electronics in Electric Utilities: HVDC Power Transmission Systems". *Proceedings of IEEE,* Vol. 76, No. 4, pp. 495-506, April 1988.

[5] J. Paulinder. "Operation and Control of HVDC Links Embedded in AC Systems". Thesis, Dept. Electric Power Engineering, Chalmers University of Technology, 2003.

[6] S. Lefebvre, J. Reeve, A. Gole, L. Pilotto, N. Martins, S. Bhattacharya. "Report on Test Systems for AC/DC Interaction Studies". *IEEE Trans. On Power Delivery*, Vol. 10, No. 4, pp. 2027-2034, Oct. 1995.

[7] P. Kundur. *Power System Stability and Control*. USA: McGraw-Hill, 1994.

[8] M. Szechtman, T. Wess, C.V. Thio, "First Benchmark Model for HVDC Control Studies", *Electra*, No. 135, pp 55-73, April 1991.

[9] MATLAB User's guide, Mathworks Inc. version 7.4.0.287 (R2007a), January, 2007.

[10] IEEE committee report, "HVDC Controls for System Dynamic Performance," *IEEE Trans.*, Vol. PWRS-6, No. 2, pp. 743-752, May 1991.

[11] S. Lefebvre, W. Wong, J. Reeve, J. Gagnon, B. Johnson, "Experience with Modeling MTDC Systems in Transient Stability Programs," *IEEE Trans. On Power Delivery*, Vol. 6, No. 1, pp. 405-413, January 1991.

[12] IEEE committee report, "Functional Model of Two-Terminal HVDC Systems for Transient and Steady-State Stability," *IEEE Trans. On Power Apparatus and Systems*, Vol. PAS-103, No. 6, pp. 1249-1255, June 1984.

[13] F. Karlecik, "A New Close Loop Control Method for HVDC Transmission," *IEEE Trans. On Power Delivery*, Vol. 11, No. 4, pp. 1955-1960, October 1996.

[14] IEEE committee report, "Dynamic Performance Characteristics of North American HVDC Systems for Transient and Dynamic Stability Evaluations," *IEEE Trans. On Power Apparatus and Systems*, Vol. PAS-100, No. 7, pp. 3356-3364, July 1981.

[15] H. Avila, G. Venayagamoorthy, and G. Olguin, "Comparison of HVDC Studies on PSCAD/EMTDC/EMTDC and SIMULINK SimPowerSystems Digital Simulation Platforms," presented at EPRI HVDC Conference, Denver-Colorado, USA, September 13-14, 2007.

[16] Å. Ekström and G. Liss, "A Refined HVDC Control System," *IEEE Trans. On Power Apparatus and Systems*, Vol. PAS-89, No. 5/6, pp. 723-732, June 1970.

[17] V. Arcidiacono, E. Ferrari, R. Marconato, J. Dos Ghali, D. grandez, "Evaluation and Improvement of Electromechanical Oscillation Damping by Means of Eigenvalue-Eigenvector Analysis ," *IEEE Trans. On Power Apparatus and Systems*, Vol. PAS-99, No. 2, pp. 769-778, April 1980.

[18] M. Aboul-Ela, A. Sallam, J. McCalley, A. Fouad, "Damping Controller Design for Power Systems Oscillations Using Global Signals," *IEEE Trans. On Power Systems*, Vol. 11, No. 2, pp. 767-773, May 1996.

[19] F. Pagola, I. Pérez, G. Verghese, "On Sesitivities, Residues and Participations: Applications to Oscillatory Stability Analysis and Control," *IEEE Trans. On Power Systems*, Vol. 4, No. 1, pp. 278-285, February 1989.

[20] D. Ostojic, "Stabilization of Multimodal Electromechanical Oscillations by Coordinated Application of Power Systems Stabilizers," *IEEE Trans. On Power Systems*, Vol. 6, No. 4, pp. 1439-1445, November 1991.

[21] N. Yang, Q. Liu, J. McCalley, "TCSC Controller Design for Damping Interarea Oscillations," *IEEE Trans. On Power Systems*, Vol. 13, No. 4, pp. 1304-1310, November 1998.

[22] R. Oliveira, R. Ramos, N. Bretas, "A Mixed Procedure Based on Classical and Modern Control to Design Robust Damping Controllers," *IEEE Trans. On Power Systems*, Vol. 22, No. 3, pp. 1231-1239, August 2007.

[23] S. Arabi, G. Rogers, D. Wong, P. Kundur, M. Lauby, "Small Signal Stability Program Analysis of SVC and HVDC in AC Power Systems," *IEEE Trans. On Power Systems*, Vol. 6, No. 3, pp. 1231-1239, August 1991.

[24] J. Guckenheimer and P. Holmes. *Nonlinear Oscillations, Dynamical Systems, and Bifurcations of Vector Fields*. Springer, February 8, 2002.

[25] J. D'Azzo. *Sistemas Realimentados de Control*. Madrid, Ed. Paraninfo, 1989.

[26] G. Rogers. *Power System Oscillations*. USA: Kluwer Academic Publishers, 2005.

[27] M. Klein, G. Rogers, P. Kundur, "A Fundamental Study of Inter-Area Oscillations in Power Systems," *IEEE Trans. On Power Systems*, Vol. 6, No. 3, pp. 914-921, August 1991.

[28] R. Cresap, D. Scott, W. Mittelstadt, C. Taylor, "Damping of the Pacific AC Intertie Oscillations Via Modulation of the Parallel Pacific HVDC Intertie," *CIGRE Paper*, 14-05, Paris, 1978.

[29] T. Embaie, D. Holmberg, U. Jonsson, E. Auranne, E. Hagman, K. Jääskeläinen, "Fenno-Skan HVDC Link as a Part of Interconnected AC/DC System," *CIGRE Int. Conf.*, 14-02, Paris, 1988.

[30] H. Breulmann, W. Winter, P. Dupuis, J. Zerenyi, J. Dudzik, L. Martin, "Analysis and Damping of Inter-Area Oscillations in the UCTE/CENTREL Power System," *CIGRE Int. Conf.*, 38-113, Paris, 2000.

[31] T. Shome, A. Gole, D. Brandt, R. Hamlin, "Adjusting Converter Controls for Paralleled DC Converters Using a Digital Transient Simulation Program," *IEEE Trans. On Power Systems*, Vol. 5, No. 1, pp. 12-19, February 1990.

[32] PSCAD/EMTDC user's guide, Manitoba-HVDC Research Center, version 4.2.1, May 2006.

[33] Task Force on Discrete Supplementary Controls, "A Description of Discrete Supplementary Controls for Stability," *IEEE Trans. On Power Apparatus and Systems*, Vol. PAS-97, No. 1, pp. 149-165, January 1978.

[34] T. Ohyama, A. Watanabe, K. Nishimura, S. Tsuruta, "Voltage Dependence of Composite Loads in Power Systems," *IEEE Trans. On Power Apparatus and Systems*, Vol. PAS-104, No. 11, pp. 3064-3073, November 1985.

[35] C. Concordia and S. Ihara, "Load Representation in Power System Stability Studies," *IEEE Trans. On Power Apparatus and Systems*, Vol. PAS-101, No. 4, pp. 969-977, April 1982.